iScience

CellPress
OPEN ACCESS

Article

Spatiotemporal Resolved Leaf Angle Establishment Improves Rice Grain Yield via Controlling Population Density

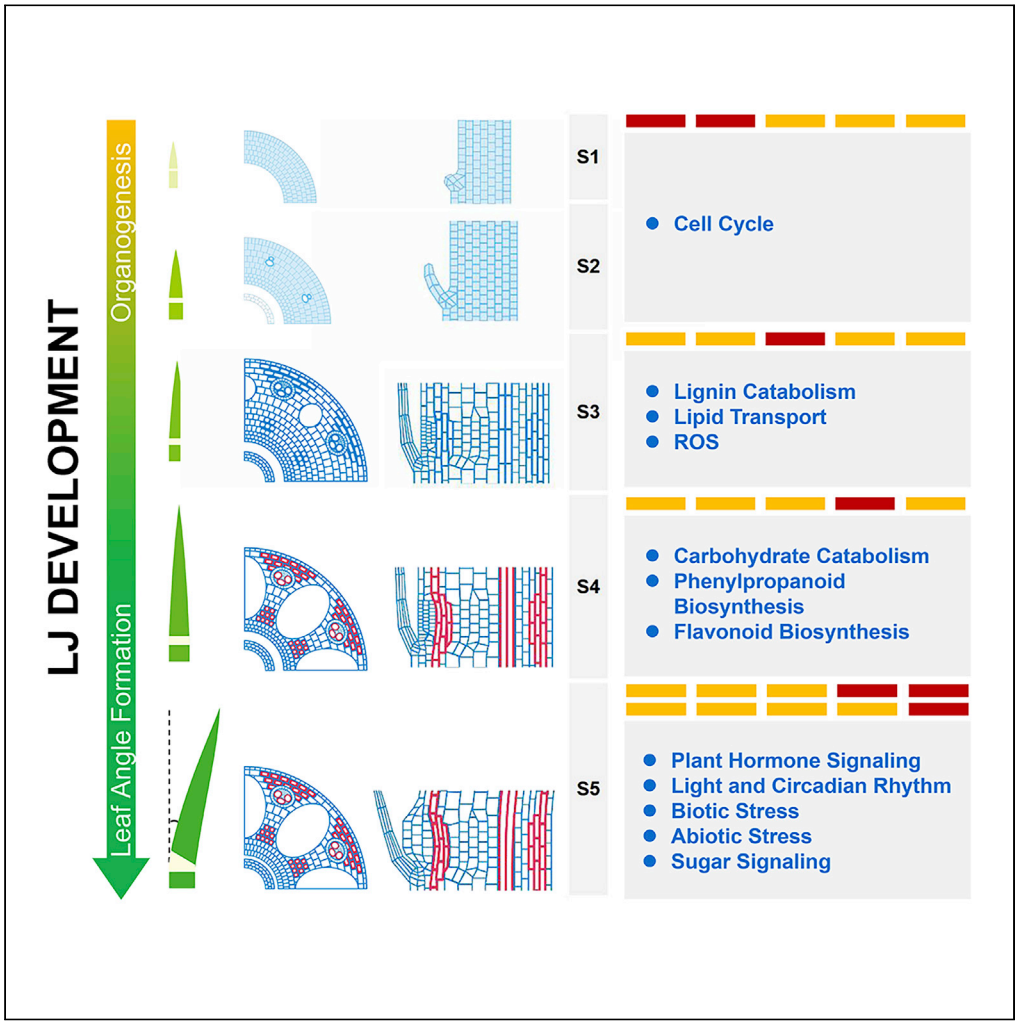

Rongna Wang, Chang Liu, Qinzhong Li, Zhina Chen, Shiyong Sun, Xuelu Wang

sunshiyong@mail.hzau.edu.cn (S.S.)
xueluw@henu.edu.cn (X.W.)

HIGHLIGHTS

The cytological dynamics of LJs from organogenesis to leaf angle formation

The dynamic mRNAs and small RNAs during LJ organogenesis and leaf angle formation

The profiles reveal how to establish cytological dynamics and leaf angle plasticity

A resource for remodeling leaf angle to enhance high-density rice yield

Wang et al., iScience 23, 101489
September 25, 2020
https://doi.org/10.1016/j.isci.2020.101489

iScience

CellPress
OPEN ACCESS

Article

Spatiotemporal Resolved Leaf Angle Establishment Improves Rice Grain Yield via Controlling Population Density

Rongna Wang,[1,2,3] Chang Liu,[1,2,3] Qinzhong Li,[1] Zhina Chen,[1] Shiyong Sun,[2,4,*] and Xuelu Wang[2,*]

SUMMARY

Leaf angle is mainly determined by the lamina joint (LJ) and contributes to ideal crop architecture for high yield. Here, we dissected five successive stages with distinct cytological features of LJs spanning organogenesis to leaf angle formation and obtained the underlying stage-specific mRNAs and small RNAs, which well explained the cytological dynamics during LJ organogenesis and leaf angle plasticity. Combining the gene coexpression correlation with high-throughput promoter analysis, we identified a set of transcription factors (TFs) determining the stage- and/or cytological structure-specific profiles. The functional studies of these TFs demonstrated that cytological dynamics determined leaf angle and that the knockout rice of these TFs with erect leaves significantly enhanced yield by maintaining the proper tiller number under dense planting. This work revealed the high-resolution mechanisms of how the cytological dynamics of LJ determined leaf erectness and served as a valuable resource to remodel rice architecture for high yield by controlling population density.

INTRODUCTION

The lamina joint (LJ), a unique organ connecting the leaf blade to the sheath in grass, consists of a collar, the ligules, and the auricles in rice (Hoshikawa, 1989). The LJ determines leaf angle dynamics by bending the leaf blade away from the vertical axis of leaf sheath, which is crucial for shaping the sessile plant architecture, and allowing optimal light capture in response to the changing environments and developmental stages (Zhu et al., 2015). Especially for the modern cereal crops, including rice, maize, and barley, the LJ is a primary determinant of leaf angle, a key trait for the high-density planting, which enhances the yields of green revolution varieties, and contributes to the future agricultural sustainability and food security (Angus et al., 1972; Sakamoto et al., 2006; Tian et al., 2019).

Cytological structures, regulated by developmental, hormonal, and environmental cues during organogenesis, generally determine LJ morphology and function (Lee et al., 2007; Li et al., 2014; Ruan et al., 2018; Sun et al., 2015; Zhang et al., 2015; Zhou et al., 2017). In rice, mature LJs contain various cytological structures, including aerenchyma, sclerenchyma, parenchyma cells, and vascular bundles (Sun et al., 2015; Zhou et al., 2017). Several studies uncovered the relationship between leaf angle and certain cytological structures in LJ, including cell wall composition, cell division, and cell elongation (Ning et al., 2011; Ruan et al., 2018; Sun et al., 2015). Meanwhile, phytohormones play important roles in regulating the leaf angle by altering the cytological structure of LJs. Brassinosteriods (BRs) regulate leaf erectness in cereals, as indicated by the decreased leaf angle of BR-deficient and BR signaling mutants and increased leaf angle in rice plants with enhanced BR biosynthesis and signaling (Bai et al., 2007; Hong et al., 2005; Yamamuro et al., 2000; Zhang et al., 2014). BR signaling controls cell elongation at the adaxial side of the rice LJ and sclerenchyma cell proliferation at the abaxial side (Sun et al., 2015; Zhang et al., 2009). Auxin plays a negative role in controlling leaf angle, as indicated by the finding that reducing auxin levels or signaling results in enlarged leaf angles by promoting parenchyma cell elongation at the adaxial sides of LJs (Zhang et al., 2015; Zhao et al., 2013). Strigolactone-deficient or strigolactone-signaling mutants exhibit enhanced leaf inclination at the seedling stage due to increased transverse cell number in the middle regions of LJs and increased longitudinal cell length in the adaxial epidermis of LJs (Li et al., 2014). In addition, environmental cues also determine the plasticity of LJs in cereals. Blue light and sufficient soil nutrients, such as nitrogen and phosphate, promote leaf bending in rice (Asahina et al., 2014; Kumagai et al., 2014; Ruan

[1]National Key Laboratory of Crop Genetic Improvement, College of Life Science and Technology, Huazhong Agricultural University, Wuhan 430070, China

[2]State Key Laboratory of Crop Stress Adaptation and Improvement, School of Life Science, Henan University, Kaifeng 475004, China

[3]These authors contributed equally

[4]Lead Contact

*Correspondence: sunshiyong@mail.hzau.edu.cn (S.S.), xueluw@henu.edu.cn (X.W.)

https://doi.org/10.1016/j.isci.2020.101489

et al., 2018), whereas phosphate deficiency leads to leaf erectness by reducing the proliferation and expansion of both sclerenchyma cells at the abaxial side and parenchyma cells at the adaxial side of the LJ (Ruan et al., 2018). Therefore, LJs may integrate diverse internal and environmental stimuli to shape optimal leaf angle, which results from the alteration of cytological structures. Finally, the presence of an intact LJ structure is essential for the dynamic regulation of leaf angle. In rice and maize, *liguleless* mutants, with the deficient auricle, ligule, and collar formation, display constantly erect leaves (Lee et al., 2007; Moreno et al., 1997; Walsh et al., 1997). Therefore, the spatiotemporal patterns of cell division, elongation, and differentiation as well as tissue formation during LJ organogenesis are crucial to determine leaf angle. However, knowledge regarding what is the cytology dynamics in LJ from organogenesis to leaf angle formation and how these structural dynamics determine leaf angle formation is still limited.

Leaf erectness, which is determined by leaf angle, is an important trait for ideal plant architecture in cereals (Donald, 1968; Khush, 1995). Erect leaves allow for better light penetration to lower leaves to increase leaf area index, which might lead to higher net photosynthesis per unit area to enhance total biomass and grain yield (Sinclair and Sheehy, 1999). Grain yield per unit area is determined by the panicle number per unit area, the grain number per panicle, and the weight of an individual grain (Beighley, 2010). Studies on the relationship between erect leaves and grain yields in barley, rice, and maize suggested that, under dense planting conditions, plants with erect leaves had higher yields than the wild-type control for various reasons: higher leaf area index and net crop photosynthesis in barley (Angus et al., 1972), higher panicle number per unit area in rice (Sakamoto et al., 2006), and lower decrease of grain yield per plant in maize (Tian et al., 2019).

In the current study, we systematically dissected the cytological dynamics in rice LJs from LJ organogenesis to leaf angle formation, explored the underlying mechanisms of how to establish the structure dynamics, and revealed how the cytological structure dynamics in LJ determined leaf angle and grain yield. Our findings provide the mechanisms, resources, and materials for remodeling rice architecture to improve yields by controlling planting density.

RESULTS

Cytological Characters of LJ from Organogenesis to Leaf Angle Formation

To explore the cytological dynamics of LJs from organogenesis to leaf angle formation, we carefully observed the second true leaf, the first complete leaf (composed of a blade, sheath, and LJ region) in rice (Hoshikawa, 1989), along a developmental trajectory after seed germination. The developmental processes were divided into five successive stages based on the morphological features of developing seedlings and LJs (Figures 1A–1J). At stage 1 (S1), on the fourth day after germination (4 DAG), the first complete leaf was fully wrapped by a coleoptile (Figure 1A), the blade length was ~2 mm, and the sheath was just emerging (Figures 1F and 1U); but the boundary between the blade and sheath was visible (Figure 1F), indicating that the LJ differentiation was initiated. At stage 2 (S2, 5 DAG), the incomplete leaf, which lacks a blade and a collar (Hoshikawa, 1989; Moldenhauer et al., 2001), grew out from the coleoptile for 2–5 mm, and the first complete leaf was still fully wrapped by the incomplete leaf (Figure 1B), whereas the LJ region was enlarged (Figures 1G and 1U). At stage 3 (S3, 6 DAG), the tip of the first complete leaf grew out from the incomplete leaf with a length of 2–5 mm, whereas the LJ of the first complete leaf was still covered by the incomplete leaf (Figures 1C and 1H). At stage 4 (S4, 7 DAG), the LJ of the first complete leaf grew out from the incomplete leaf (Figures 1D and 1I) with fully elongated blade (Figure 1U). At stage 5 (S5, 9 DAG), the expanded blade of the first complete leaf bent away from the vertical axis to form leaf angle (Figures 1E and 1J).

Then we documented the cytological structures of developing LJs during the five stages by carefully observing both transverse and longitudinal sections (Figures S1 and 1K–1T). At S1, all cells in LJs contained dense cytoplasm and a large nucleus and the ligule was growing out from the adaxial epidermis via periclinal cell division (Figures 1K and 1P). At S2, vascular bundles were differentiating (Figure 1L) and the ligule protruded via cell proliferation (Figure 1Q). At S3, dramatic changes in LJ development occurred, as indicated by the active differentiation of tissues, including aerenchyma, xylem, phloem, and sclerenchyma cells, but with less lignin deposition on the cell wall (Figures 1M and 1R). In addition, the cell size and cell number significantly increased from S1 to S3 (Figures 1V and 1W). Notably, lignin accumulation was apparently observed at S4 (Figures 1N, 1S, 1O, and 1T) and leaf angle formed at S5 (Figures 1E and 1J), which was accompanied by the expanded and elongated parenchymal cells at the adaxial side of LJ

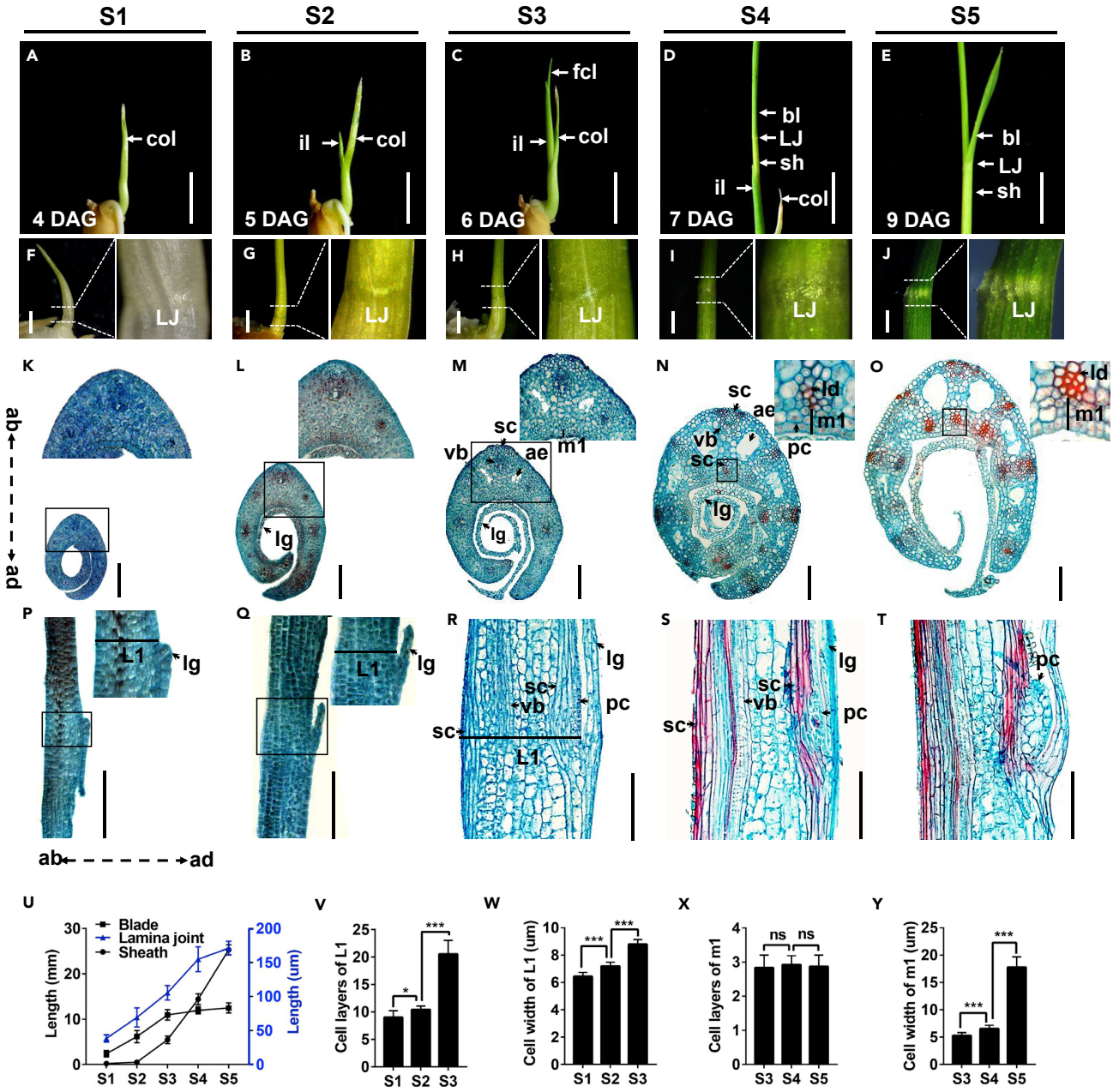

Figure 1. Successive Changes in Morphology and Anatomy of Developing LJs

(A–E) Seedling morphology at five stages during LJ development (S1–S5). col, coleoptile; il, incomplete leaf (the first true leaf); fcl, first complete leaf (the second true leaf); LJ, lamina joint; bl, blade; sh, sheath; DAG, days after germination. Scale bars, 0.5 cm.

(F–J) LJ morphology of the first complete leaf at five stages shown in (A-E). The left panel, the phenotype of LJ region in the first complete leaf; the right panel, the magnified view of LJ in the first complete leaf. LJ, lamina joint. Scale bars, 0.2 mm.

(K–T) Cross sections (K–O) and longitudinal sections (P–T) of the LJs in the first complete leaves at five stages. lg, ligule; vb, vascular bundle; sc, sclerenchyma; ae, aerenchyma; pc, parenchyma; ab, abaxial side; ad, adaxial side; ld, lignin deposition. m1, the region between the adaxial sclerenchyma and the adaxial epidermis in a cross section; L1, the region between the abaxial and the adaxial epidermis in a maximum longitudinal section. The upper images are magnified views of the regions indicated in black boxes. Scale bars, 100 μm.

(U) Lengths of LJs, blades, and sheaths of the first complete leaves at five stages (n = 10).

(V and W) Cell layers (V) and cell width (W) in the L1 regions (P–R). (n = 10).

(X and Y) Cell layers (X) and cell width (Y) in the m1 regions (M–O). (n = 10).

Data are the means ± standard deviation (SD). Significance of all comparisons was determined using Student's t test with *$p < 0.05$, **$p < 0.01$, ***$p < 0.001$, and ns indicates no significance. See also Figure S1.

without increased cell number (Figures 1O, 1T, 1X, and 1Y). Therefore, the basic cytological structures of the LJ formed from S1 to S4, without leaf blade bending, whereas from S4 to S5, the leaf blade bent away to form leaf angle. It is indicated that leaf angle might be determined by the balance between the pushing force from the expanding parenchymal cells at the adaxial side of the LJ and the supporting force from the basic structure of the LJ. Taken together, our cytological dissection of the five stages of LJs and leaf angle formation captured the dynamic transitions of LJ development.

The Dynamic mRNA Transcriptomes of Developing LJs

To reveal the dynamic regulatory networks during LJ development, we performed mRNA sequencing using RNA samples from LJs and blades at five stages (Figure S2). We obtained 25.1–41.7 million reads per library (Table S1), which were aligned to 34,679 genes using the rice reference genome (IRGSP-1.0) (Table S2) and were expressed in at least one sample (FPKM > 0, FPKM: fragments per kilobase of transcript per million reads). Principle-component analysis of the 20 libraries revealed two main sources of variability among the data (Figures S3A and S3B; Table S2). The main principle component (PC1) explained 56.22% of the variance and separated samples of S1–S3 from that of S4–S5 (Figure S3B). The genes in the S1–S3 samples are mainly involved in translation, cell component biogenesis and assembly, cell cycle, and cell division (Figure S3C), which is consistent with the cytological characters of LJs at S1–S3. The second principle component (PC2) explained 17.19% of the variance and separated the samples of S3–S4 from that of S1–S2 and S5 (Figure S3B). The genes enriched in the S3 and S4 samples mainly function in cell wall organization (Figure S3C), which is consistent with the finding that secondary cell wall formation and lignin biosynthesis primarily occur during S3 and S4. In general, the genes in each sample are highly diverse with stage-specific identities during LJ development (Figure S3D).

In total, we identified 19,162 differentially expressed genes (DEGs) from the comparisons between any two LJ samples at different stages, which were further classified into 23 distinct clusters with stage-specific expression patterns (Table S2). Importantly, 41.8% of the DEGs (8,008 genes) were mainly expressed at a single stage (Figure 2A, cluster M01 to M05) and 52.9% of the DEGs (10,139 genes) were expressed at two or more successive stages (Figures 2A and S4A, cluster M06, M10, M12, M14, M15, M19, M20, and M21). Using gene ontology (GO) enrichment analysis, we observed that these genes dominantly expressed at S1 (cluster M01), S2 (cluster M02), or both (cluster M06) primarily participate in translation and the cell cycle (Figures 2B and S4B), which explained the active cell division observed in LJs at S1 and S2 (Figures 1K, 1L, 1P, and 1Q). To further evaluate the stage specificity of our RNA samples, we observed the expression patterns of previously reported genes involved in LJ boundary formation (*KNOX*) (Postma-Haarsma et al., 2002; Tsuda et al., 2014), ligule initiation (*OsYAB3* and *OsROC1*) (Dai et al., 2007; Ito et al., 2002), and cell number regulation of LJ vascular bundles (*OsLIC*) (Wang et al., 2008). These genes were highly expressed at S1 and/or S2 (Figures 2C and 2D). The enriched GO terms for the genes in cluster M03, including "response to oxidative stress" and "lignin catabolism," are associated with monolignol production for lignin polymerization (Bao et al., 1993; Quiroga et al., 2000). The enriched GO terms for genes in cluster M04 (Figures 2B and S5), including "carbohydrate catabolism," "aromatic amino acid family metabolism," "phenylpropanoid biosynthesis," and "flavonoid biosynthesis," are likely involved in component deposition for secondary cell wall formation (Besseau et al., 2007; Tzin et al., 2010; Vogt et al., 2010). These findings indicate that lignin biosynthesis initiates at S3 and that lignin deposition and secondary cell wall formation primarily occurs at S4, which are consistent with the cytological characters of LJs at S3 and S4 (Figures 1M, 1N, 1R, and 1S). The reported genes that regulate sclerenchyma cell (*OsCYC U4;1*) (Sun et al., 2015) and cellulose content (*OsILA1*) (Ning et al., 2011) were specifically expressed in cluster M03 and M04, respectively (Figure 2E). In addition, several genes enriched in the GO term "response to oxidative stress" in cluster M03, encoding reactive oxygen species-scavenging proteins that trigger programmed cell death (PCD) (del Rı'o et al., 2002; Hu et al., 2011), might be responsible for aerenchyma initiation during S3 (Figure 1M). Several known genes that function in PCD (Hatsugai et al., 2015; Lam et al., 2000) were highly expressed at S3–S5 (Figures 2G and 2H), further supporting the notion that PCD plays important roles in aerenchyma formation from S3 to S5. Remarkably, the enriched GO terms at S5 (cluster M05) and S4–S5 (cluster M14) were mainly involved in responses to multiple signals, including plant hormones, light, circadian rhythm, biotic and abiotic stresses, nutrients (phosphorus, sugar, nitrogen), and general signaling components (Figures 2I and 2J; Table S3). Because the major feature of LJs at S5 is the cellular expansion at the adaxial side of the LJ to form leaf angle (Figures 1E, 1J, 1O, and 1T), the integration of diverse internal and external stimuli to determine the final leaf angle may be dependent on the cellular expansion at the adaxial side of the LJ. Consistent with the suggestion, BR, auxin, light, and gravitropism signals have been reported to

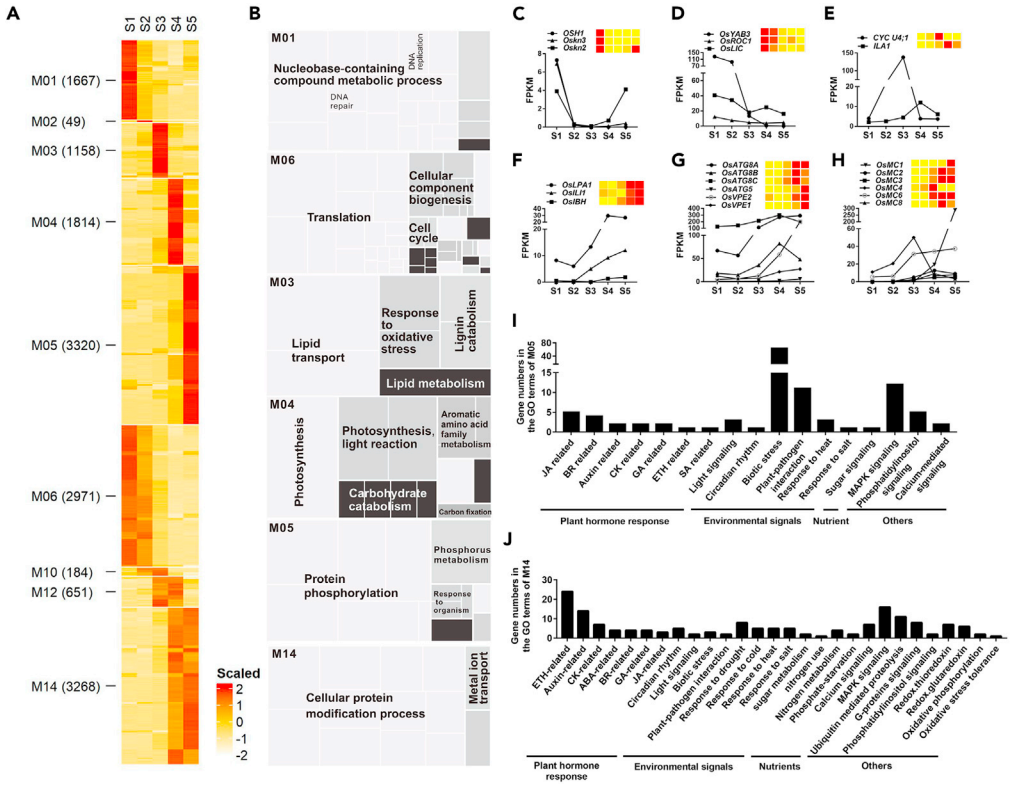

Figure 2. Dynamic mRNA Transcriptomes in Developing LJs

(A) Main clusters of DEGs in LJs at five stages of development. Heatmaps show the expression patterns of genes. The expression values were normalized using the *Z* score method; the number of genes in each cluster is indicated in brackets.

(B) Functional categories enriched by GO analysis (false discovery rate $\leq$0.05) were summarized using REVIGO for clusters M01, M06, M03, M04, M05, and M14. The related GO terms are displayed in similar colors; the aggregate size indicates the significance of the GO terms.

(C–H) Expression patterns of the genes reported to function in regulating the cytological structures of LJs (C–F) and in the PCD process (G and H). The FPKM values and the normalized expression values at five stages are shown. Heatmaps represent the normalized expression values determined using the *Z* score method.

(I and J) The diverse signals are indicated by genes from the enriched GO terms in cluster (I) M05 and (J) M14.

See also Figures S4 and S5.

regulate leaf angle via cell elongation in the adaxial epidermis (Asahina et al., 2014; Wu et al., 2013; Zhang et al., 2009, 2015; Zhao et al., 2013), and several known genes involved in these signals were specifically expressed at S4 and S5 (Figure 2F). Taken together, these results suggest that our transcriptomes well explained the stage-specific characters of LJs.

Dynamic miRNA Profiles during LJ Development

Several microRNAs (miRNAs) have been reported to regulate leaf angle in rice (Bian et al., 2012; Gao et al., 2018; Zhang et al., 2013), but the regulatory networks of miRNAs that function in LJ development and leaf angle are still unknown. Using the same samples used for mRNA profiling, we performed small RNA sequencing (RNA-seq) by BGISEQ-500 and obtained 20.4–22.8 million reads per library with an average mapping rate of 84.5% (Table S1). The most abundant reads in all libraries were 21-nucleotide (nt) and 24-nt small RNAs (sRNAs); the 24-nt sRNAs contained more distinct sequences than the others (Figure S6). Using shortstack for *de novo* annotation of *MIRNA* loci (Axtell, 2013), we identified 200 *MIRNAs* loci (Table S4). Among these loci, 141 are recorded in miRBase (http://www.mirbase.org) and the 59 other loci are not recorded in miRBase, including three loci assigned to known miRNA families (Figure 3A). In addition, 56 known *MIRNA* loci in our data produced variants of mature miRNAs (termed isomiRs) (Figure 3A). Among these, 20 isomiRs were derived from another arm of the pre-miRNAs and the others were derived from the same arm as the reported ones, but with 3′ or 5′ end variations or from altered positions (Table S4).

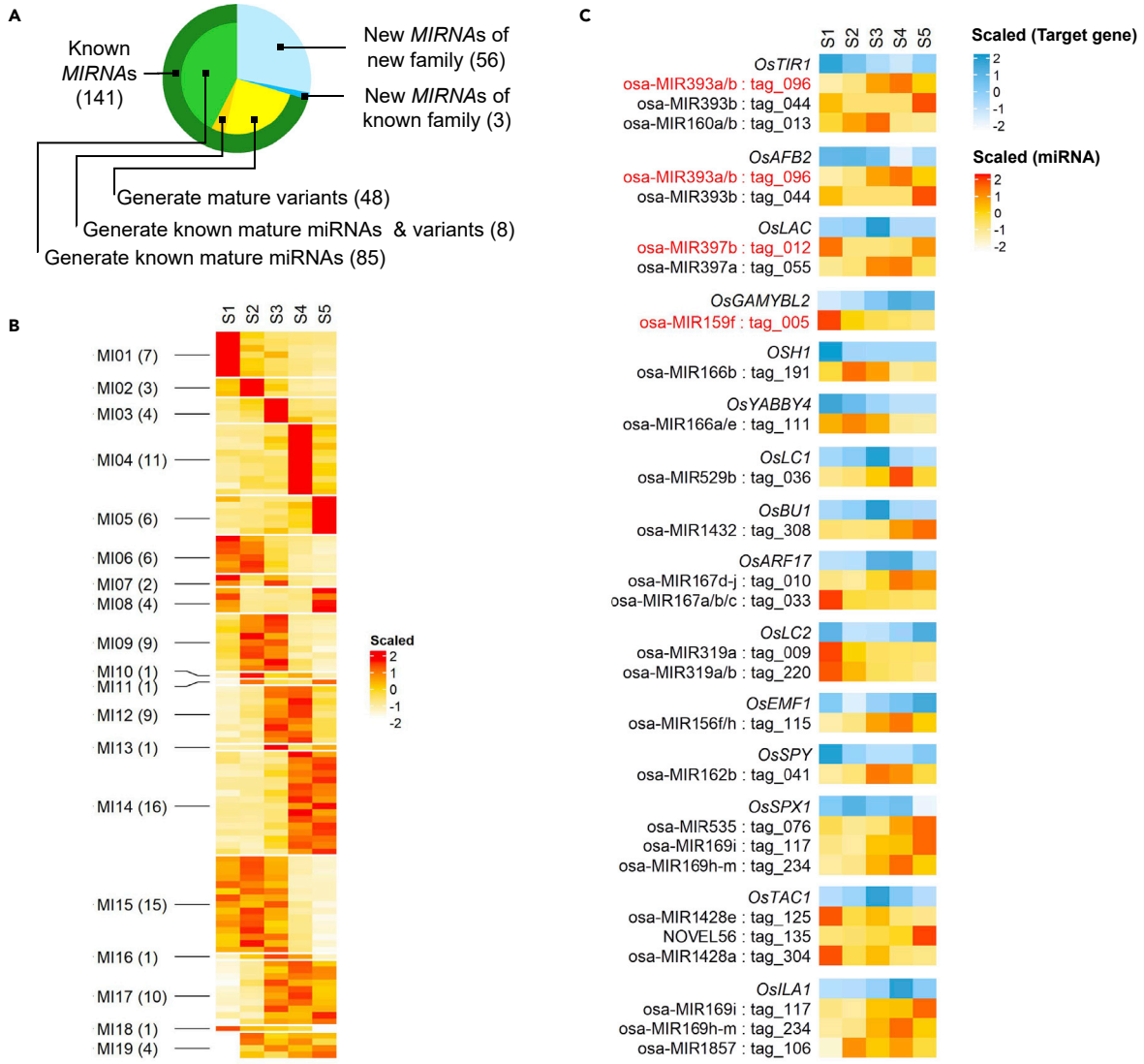

Figure 3. Dynamic miRNA Profiles and their Predicted Targets in Developing LJs

(A) Classification of *MIRNA* loci by *de novo* annotation. The subsets of these loci indicate the types of mature miRNAs identified in our data. The number of *MIRNA* loci is indicated in brackets.

(B) Clusters of DEMs in LJs at five stages. The expression values (RPM) were normalized using the *Z* score method; the number of miRNAs in each cluster is indicated in brackets.

(C) Predicted miRNA-target pairs that function in leaf angle regulation. Heatmaps show the expression patterns of miRNAs and their predicted targets known to function in leaf angle regulation. The miRNAs in red are miRNA-target pairs known to regulate leaf angle.

See also Figure S7.

Furthermore, we identified 185 distinct mature miRNAs from 200 *MIRNA*s loci, including 77 miRNAs recorded in the miRBase and 108 miRNAs not in the miRBase (Figure S7A; Table S4). However, 299 reported mature miRNAs in rice (recorded in miRBase) were not identified as major sRNAs within known loci, but were present in our libraries (Figure S7B) and might play roles in LJ development (Lu et al., 2008). Therefore, to avoid missing these miRNAs, we performed quantification and differential expression analysis (false discovery rate $\leq$0.05; maximum expression value $\geq$5 RPM) of all miRNAs detected in all samples.

In total, we identified 111 differentially expressed miRNAs (DEMs) between any pairwise combination among the LJ samples at five stages, including 82 known miRNAs and 29 miRNAs that are not recorded in miRBase (Table S5), and clustered them into 19 stage-specific modules (Figure 3B), indicating the potential roles of DEMs in determining the stage-specific characters of LJs. To reveal the functions of these stage-

specific DEMs, we used psRNATarget (Dai and Zhao, 2011) and identified 220 target genes from the DEGs set during LJ development (expectation ≤2.5; Table S5). These target genes were enriched in GO terms of phenylpropanoid/lignin catabolic process, secondary metabolism, transcription, auxin response, and circadian rhythm (Figure S8). Importantly, besides the reported miRNA-target pairs that function in leaf angle regulation (Figure 3C), including osa-miR393-*OsTIR1* (Bian et al., 2012), osa-miR393-*OsAFB2* (Bian et al., 2012), osa-miR397-*OsLAC* (Zhang et al., 2013), and osa-miR159-*OsGAMYBL2* (Gao et al., 2018), we also predicted some potential pairs targeting the reported genes with the function in leaf angle regulation (expectation ≤5) (Figure 3C), including *OSH1* (Tsuda et al., 2014), *OsYABBY4* (Liu et al., 2007), *OsLC1* (Zhao et al., 2013), *OsBU1* (Tanaka et al., 2009), *OsARF17* (Chen et al., 2018), *OsLC2* (Zhao et al., 2010), *OsEMF1* (Liu et al., 2018), *OsSPY* (Shimada et al., 2006), *OsSPX1* (Ruan et al., 2018), *OsTAC1* (Ku et al., 2011), and *OsILA1* (Ning et al., 2011). In addition, some reported pairs involved in other developmental processes were also identified in our analysis (Table S5), including *OsSPL14*, which increases the number of vascular bundles and sclerenchyma cells in rice culms (Jiao et al., 2010) and *OsPCF6* and *OsTCP21*, which enhance cold stress tolerance (Wang et al., 2014). Moreover, 276 miRNA-target pairs were predicted in this study that have not been reported previously, suggesting that they might play roles in regulatory network for LJ development and leaf angle formation.

Global Identification of Key Transcription Factors Determining the Stage-Specific Characters of LJs

The aforementioned results suggest that the stage-specific transcriptomes sufficiently explained the characters of cytological dynamics during LJ organogenesis and leaf angle formation. Therefore, we used these transcriptomic data as a resource and combined the gene coexpression correlation with high-throughput promoter analysis to globally identify key transcription factors (TFs), which determine the stage- and/or cytological structure-specific patterns of small RNAs and mRNAs (Figures 4A and S9) (Yu et al., 2015; Zhan et al., 2015). Totally, we identified 46 candidate TFs determining the stage- and/or cytological structure-specific mRNAs patterns (Figures 4B–4G, Table S6), which are involved in the AP2/ERF, MADS-box, and C2H2 zinc finger families. Five of these TFs with known function, including *Os03g0215400* (*OsMADS1*) (Prasad et al., 2005), *Os01g0726400* (*CF O 1/MADS32*) (Sang et al., 2012), *Os06g0604000* (*OsWR2*) (Zhou et al., 2013), *Os05g0203800* (*OsMADS58*) (Chen et al., 2015), and *Os07g0605200* (*OsMADS18*) (Fornara et al., 2004), were not reported to directly regulate LJ and leaf angle formation, but the biological processes they regulated are involved in LJ development. For example, *Os06g0604000* (*OsWR2*), which was identified from gene cluster of M03 and the biological processes of lignin catabolism, has been reported to affect wax and cutin content in rice leaves (Zhou et al., 2013), and its ortholog in *Arabidopsis*, *AtSHN2*, was reported to function in cell wall cellulose and lignin biosynthesis in culms (Ambavaram et al., 2011); *Os05g0203800* (*OsMADS58*), predicted from the gene cluster of M03 and GO term lipid transport, has been reported to inhibit chloroplast development in rice stamen development (Chen et al., 2015), perhaps (at least partially) explaining the white color of LJs. Notably, 41 candidate TFs were first identified and may play roles in LJ development and leaf angle formation. In addition, we identified 31 candidate TFs that might determine the stage-specific patterns of miRNAs during LJ and leaf angle formation (Figures S9 and S10; Table S6). Compared with the candidate TFs determining the stage-specific mRNA pattern, there are 20 TFs in overlap, and 11 TFs specifically determined the stage-specific miRNA pattern (Table S6), including one reported gene, *Os05g0139100* (*OsPIL16/APG*) identified from the MI03 cluster, which functions in leaf angle regulation (Heang and Sassa, 2012).

The Cytological Dynamics of LJs Determine Leaf Angle Formation

To further demonstrate that the stage-specific transcriptome patterns and/or the stage-specific cytological dynamics determine the leaf angle in general, we selected a number of representative genes from the aforementioned candidate TFs responsible for the main biological processes at each stage and generated the knockout (KO) lines using CRISPR-Cas9 (Gao and Zhao, 2014; Figure S11). First, we knocked out *Os01g0922800* (named *LJS1-1*) and *Os06g0181700* (*LJS1S2-1*), identified from cluster M01 and the GO term cell cycle in M06, respectively, as well as their close homologs (*Os08g0531900*, *LJS1-1L*; *Os02g0797100*, *LJS1S2-1L*) (Figures 5A, S11A, and S11B). All these KO lines displayed erect leaves (Figures 5B and 5C), with more cell layers in L1 compared with the wild-type (Nipponbare; Ni) (Figures 5E–5H). In addition, in the LJs of the line *LJS1S2-1-cri/LJS1S2-1L-cri*, the predicted target genes in the GO term cell cycle with positive roles in cell division were up-regulated, whereas genes with negative roles in the cell cycle were down-regulated compared with the wild-type line Ni (Figure S12A) (Yuan et al., 2004; Kirik et al., 2007), indicating that they inhibits cell division during the early stages of LJ formation.

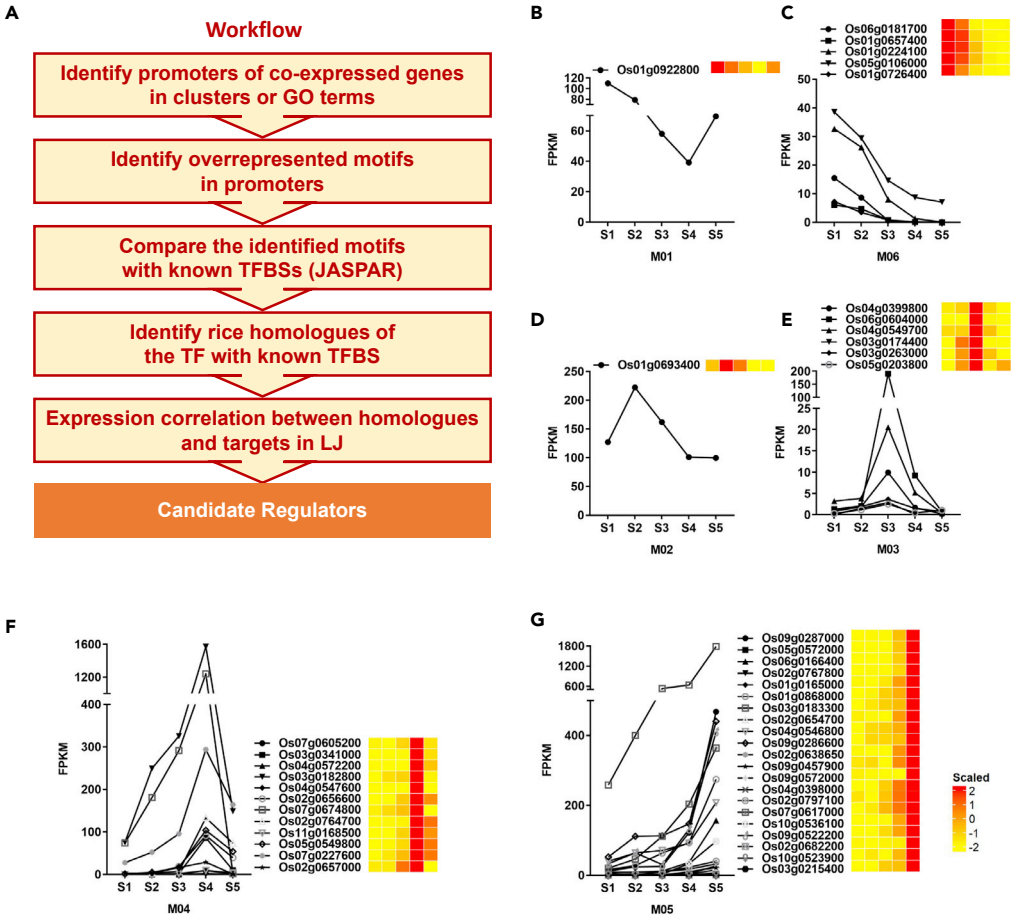

Figure 4. *De Novo* Identification of Key TFs that Potentially Determine Stage-Specific Gene expression and the identity of developing LJs

(A) Workflow used to identify the key TFs involved in LJ development.

(B–G) Key TFs identified from transcriptomes to determine the stage-specific characters of LJs. (B), Key TFs in B-G were identified from the gene cluster of M01 (B), M06 (C), M02 (D), M03 (E), M04 (F), M5 (G) respectively. The FPKM and normalized expression values at five stages are shown. Heatmaps show the normalized expression values determined using the *Z* score method.

See also Figures S9 and S10.

Second, because dramatic changes in cytological structure and gene expression occur during the S3–S4 transition of LJ development, and lignin biosynthesis and deposition on cell wall are important characteristics of S3 and S4 (Figures 1M, 1N, 1R, 1S, and 2B), we evaluated the functions of several key TFs predicted from the lignin-related GO terms during S3 and S4, including *Os04g0549700* (*LJS3-1*), *Os02g0656600* (*LJS3-1L*), *Os03g0182800* (*LJS4-1*), and *Os07g0674800* (*LJS4-2*) (Figure 5I). All KO lines of these genes exhibited decreased leaf angle in all leaves and contained more lignin on sclerenchyma cells in the LJs compared with Ni (Figures 5D, 5J, and 5K). We then measured the expression levels of the predicted target genes enriched in lignin-related GO terms. The target genes with positive roles in lignin biosynthesis were up-regulated, whereas the target genes that function in flavonoid biogenesis (with the negative roles for lignin biosynthesis) were down-regulated in the LJs of these KO lines (Figures S12B–S12D) (Besseau et al., 2007; Vogt, 2010). These results indicate that these genes determine leaf angle via negative regulation in lignin biosynthesis and lignin deposition in LJs at S3–S4.

Finally, because the dominant cytological character at S5 is the expansion of parenchymal cells at the adaxial sides of LJs, which can result in leaf angle formation (Figures 1E, 1J, 1O, and 1T), we examined the functions of two TFs *Os06g0166400* (*LJS5-1*), *Os10g0536100* (*LJS5-2*) and its homolog *Os03g0122600* (*LJS5-2L*), which were identified from cluster M05 and the GO term "cellular protein

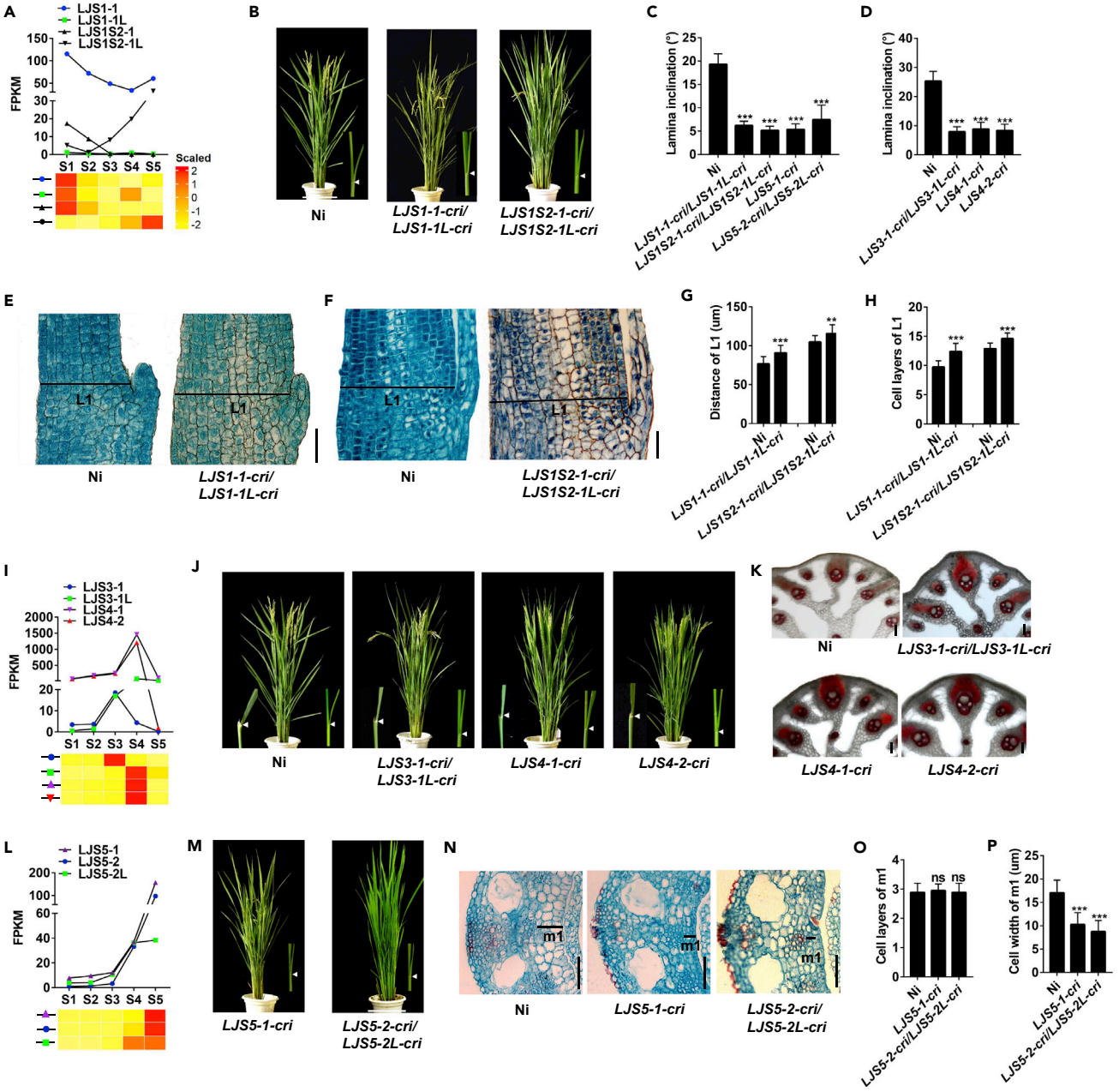

Figure 5. The Identified TFs Determine LJ Development and Leaf Angle

(A, I, and L) FPKM values and expression patterns of candidates in LJs at five stages. The TFs function at S1-S2 in (A); the TFs function at S3-S4 in (I); the TFs function at S5 in (L).

(B) Phenotypes of *LJS1-1-cri/LJS1-1L-cri*, *LJS1S2-1-cri/LJS1S2-1L-cri*, and Ni (wild-type) at the heading stage (70 DAP). The photographs on the right show the LJs of the first complete leaves at S5 (9 DAG). The arrowheads point to the locations of LJs. DAP, days after planting; DAG, days after germination.

(C) Leaf angles of the first complete leaves at the seedling stage in (B) and (m). (n = 15).

(D) Leaf angles of the flag leaf at the heading stage in (J). (n = 15).

(E and F) Longitudinal sections of LJs in the first complete leaves of *LJS1-1-cri/LJS1-1L-cri* (4 DAG, S1) (E), *LJS1S2-1-cri/LJS1S2-1L-cri* (5 DAG, S2) (F), and wild-type Ni. L1, the region between the abaxial and the adaxial epidermis in the longitudinal section of the LJ. Scale bars, 100 μm.

(G and H) The (G) distance and (H) cell layers in L1 shown in (E) and (F). (n = 15).

(J) Phenotypes of *LJS3-1-cri/LJS3-1L-cri*, *LJS4-1-cri*, *LJS4-2-cri*, and Ni at the heading stage (70 DAP). The photographs on the left show the LJs of flag leaves at 70 DAP. The photographs on the right show the LJs of the first complete leaf at 9 DAG. The arrowheads point to the locations of LJs.

(K) Phloroglucinol-HCl staining of hand-sectioned fresh LJs in flag leaves in (J). The lignin is stained in red. Scale bars, 100 μm.

Figure 5. *Continued*

(M) Phenotypes of *LJS5-1-cri*, *LJS5-2-cri/LJS5-2L-cri*, and Ni at the heading stage (70 DAP) and seedling stage (9 DAG, S5). The photographs on the right show the LJs in the first complete leaf. The arrowheads point to the locations of LJs.

(N) Cross sections of LJs in the first complete leaves at S5 in (M). m1, the region between the adaxial sclerenchyma and the adaxial epidermis in the cross sections. Scale bars, 100 μm.

(O and P) (O) Cell layers and (P) cell width of m1 shown in (N). (n = 9).

Data are the means ± SD. Significance of all comparisons was determined using Student's *t*-test with $^{**}p < 0.01$, $^{***}p < 0.001$, and ns indicates no significance. See also Figures S11 and S12.

modification process" in M14, respectively (Figure 5L). KO lines of these genes showed smaller leaf angle and decreased cell length in m1 compared with the wild-type Ni (Figures 5C and 5M–5P), suggesting that they might integrate diverse signals to regulate leaf inclination. Taken together, these results suggest that the stage-specific cytological structures in LJs generally determine leaf angle formation and significantly demonstrate that our transcriptome data and the method for key TFs prediction are the effective resource to facilitate global remodeling of leaf angle in rice.

Erect Leaves Enhance Rice Yield

To evaluate whether and/or how erect leaves affect rice yields, we planted KO rice lines with reduced leaf angle, including *LJS1-1-cri/LJS1-1L-cri*, *LJS1S2-1-cri/LJS1S2-1L-cri*, *LJS3-1-cri/LJS3-1L-cri*, *LJS4-1-cri*, *LJS4-2-cri*, *LJS5-1-cri*, and *LJS5-2-cri/LJS5-2L-cri*, using two planting densities (Sakamoto et al., 2006) to investigate yields in paddy trials in Wuhan, China, in 2019 (Figure S13A). These materials not only had increased grain yields compared with the wild-type under dense planting but also had improved yields compared with themselves and the wild-type under normal planting. Notably, although the tiller number per plant was reduced in all KO and wild-type Ni under dense planting (44.4 plants m^{-2}) versus normal planting (22.2 plants m^{-2}) (Figure S13B), the reduction of primary tiller number per plant was less in these KO lines than the wild-type under dense planting (Figure 6A), leading to significantly more primary tillers and fertile panicles per square meter in the KO rice than that in Ni under dense planting (44.4 plants m^{-2}) (Figures S13C and 6B). The 1,000-grain weight and panicle length were not strongly affected by planting density (Figures 6C and S13D). Finally, we found that the theoretical population grain yield in both the KO line and the wild-type Ni was significantly higher under the high planting density than under normal density (Figure 6D). Moreover, the grain yield of the KO lines under dense planting was markedly higher than that in the wild-type Ni under both dense and normal planting (Figure 6D). These results suggest that the rice with erect leaves has improved yield potential under dense planting, which primarily results from the reduction of the inhibited tillering under dense planting.

DISCUSSION

In the current study, the distinct cytological dissections and small RNA/mRNA profiles in LJs, which are obtained from LJ organogenesis to leaf angle formation, enable us to globally uncover the mechanisms of how to build the cytological dynamics at each stage and how to establish the leaf angle by these structures dynamics (Figure 7). Using these data as a resource, we employed an improved method and identified a set of TFs determining the stage-specific cytological structures, which can determine the leaf angle formation and enhance grain yield. In addition, considering the important roles of small RNA in leaf angle formation, we first established the global network of miRNAs and their predicted targets from the LJ organogenesis to leaf angle formation. Moreover, the LJ-specific genes that are highly expressed in LJs compared with leaf blades at each stage (Figure S14) provide an excellent promoter resource for directionally remodeling LJ to improve plant architecture.

Analysis of the cytological structure of LJs and their transcriptomes revealed that diverse signals are integrated at S4–S5 to dynamically regulate leaf blade inclination to form leaf angle, providing a genetic and molecular basis for understanding how leaf angle is dynamically regulated to help sessile plants to adapt to different developmental status and changing environments. Until S4, the leaves are still erect, without leaf angle formation, although the underlying cytological structures of LJs have been completely established (Figures 1D, 1I, 1N, and 1S). At S5, the leaf blade bends away to form leaf angle, and the most obvious change in cytological structure is the cell expansion at the adaxial side of the LJ (Figures 1E, 1J, 1O, 1T, 1Y, and 1Z). Therefore, the final leaf angle might be largely determined by the balance between cellular expansion at the adaxial side of the LJ and the mechanical support provided by LJ basic structures. Consistent with this hypothesis, most genes are known to regulate leaf angle by altering cellular expansion at the

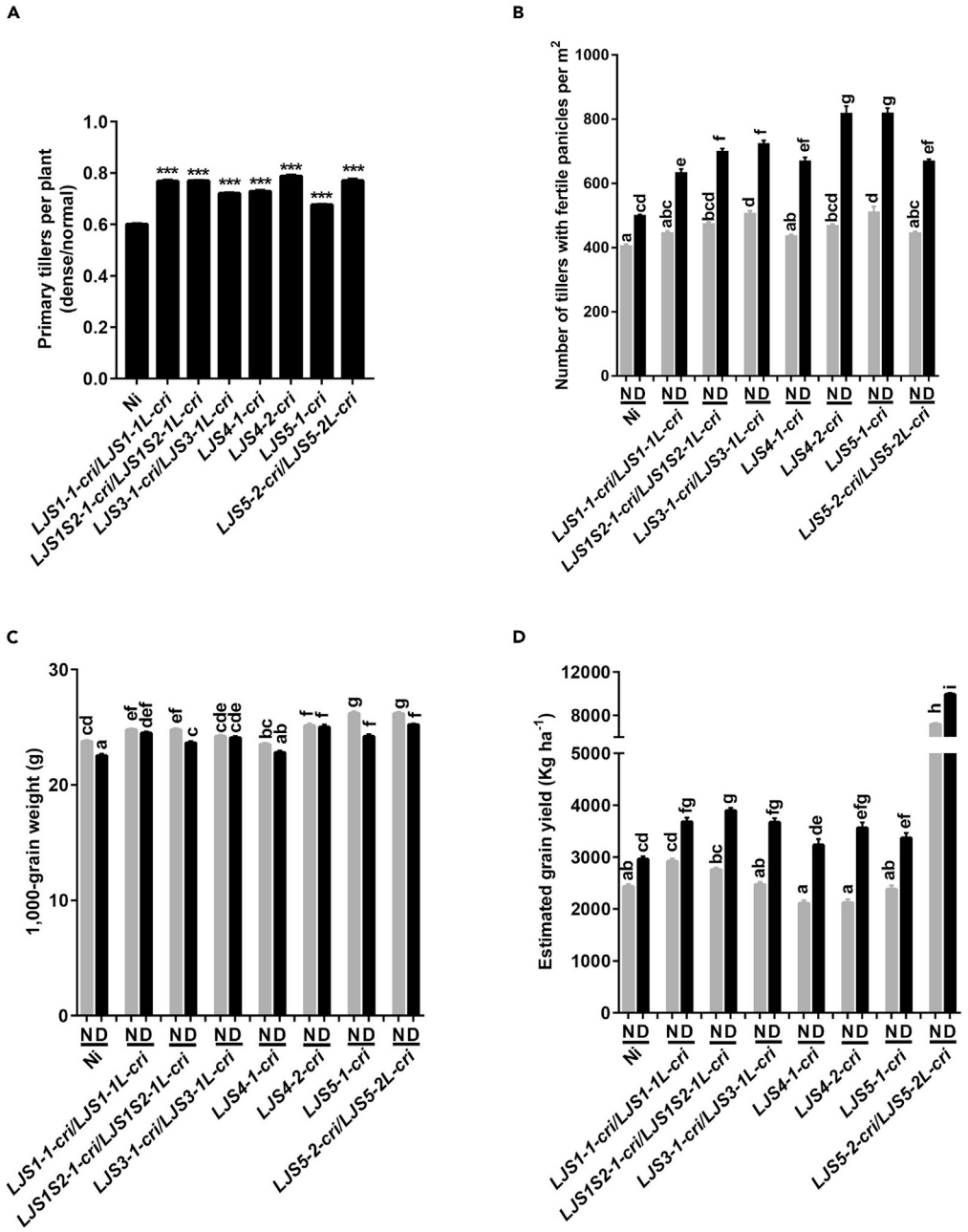

Figure 6. Rice Plants with Erect Leaves Show Enhanced Grain Yields via Dense Planting

(A) Sensitivity of tiller number per plant to planting density. Planting densities include normal planting (22.2 plants m^{-2}) and dense planting (44.4 plants m^{-2}). Data are the means ± SE (n = 40 plants). Significance was tested using Student's t test with ***$p < 0.001$.

(B) Number of tillers with fertile panicles per square meter under different planting densities.

(C) 1000-grain weight under different planting densities. n = 40.

(D) Estimated grain yields per hectare under different planting densities. ha, hectare.

(B–D) N: normal planting (22.2 plants m^{-2}); D: dense planting (44.4 plants m^{-2}).

Data are the means ± SE. Lowercase letters indicate significant differences at the level of $p < 0.05$ within a parameter (Tukey's honest significant difference test). See also Figure S13.

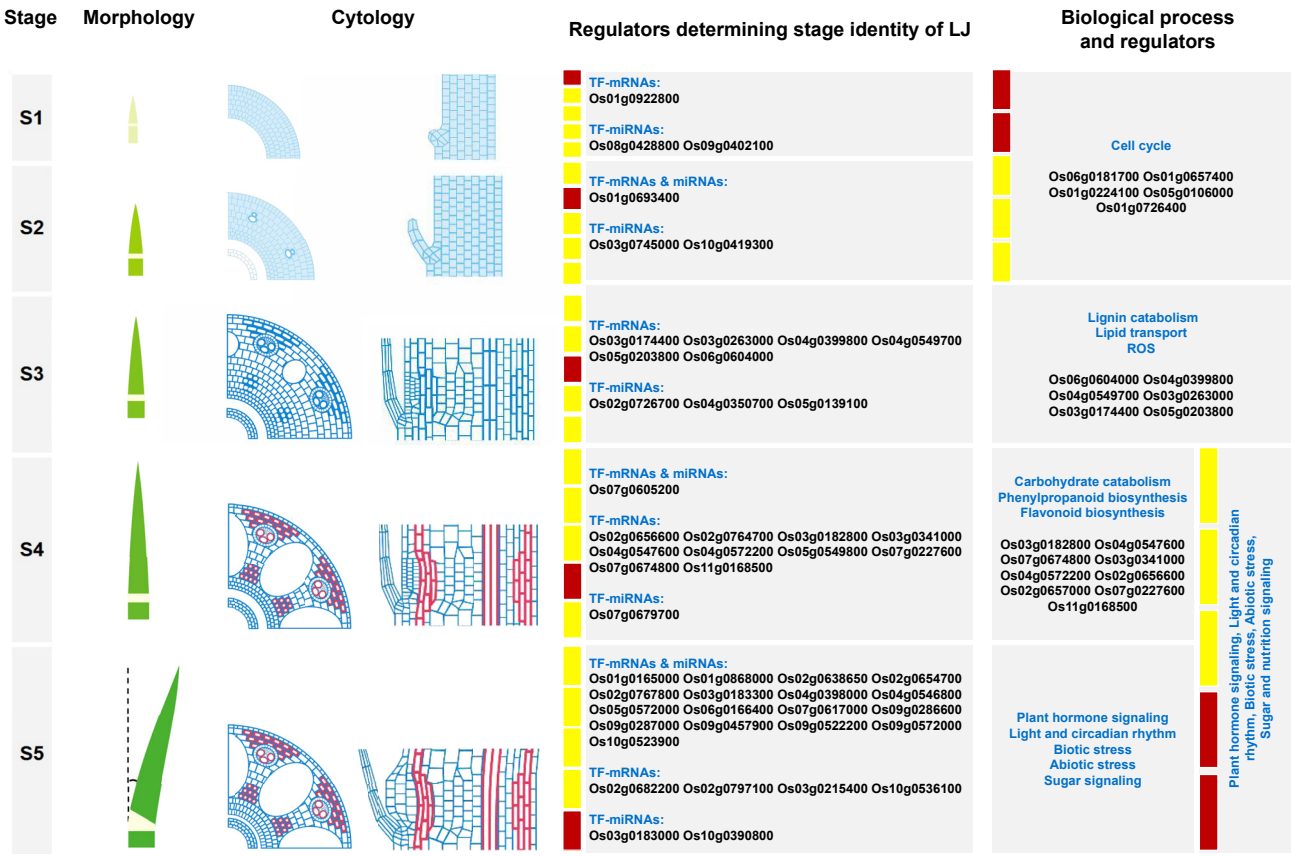

Figure 7. Schematic Model for LJ Organogenesis and Leaf Angle Formation

The model shows the key TFs that determine LJ stage-specific identities and the key biological processes involved at each stage. The red color in the panel "cytology" indicates cells with lignin disposition.

adaxial side, mechanical tissues, or both (Chen et al., 2018; Ning et al., 2011; Ruan et al., 2018; Sun et al., 2015). In addition, the degrees of leaf angles of different leaves in plants normally are not uniform, and the angle of a certain leaf dynamically changes from the vegetative to reproductive stages (Zhou et al., 2017), pointing to the plasticity of leaf angle regulation during the late stages of LJ development. The highly enriched GO terms from the stage-specific transcriptomes at S5 (M05) and S4–S5 (M14) are all related to the processes involved in protein modification, and these genes in the GO term participate in responses to diverse signals, including plant hormones, environmental stimuli, and nutrients. Among these signals, BRs, auxin, light, and phosphorus have been reported to regulate leaf angle through cell elongation in the adaxial side of the LJ (Asahina et al., 2014; Ruan et al., 2018; Zhang et al., 2009, 2015). However, other signals, including circadian rhythm, biotic stresses, heat, salt, sugar, MAPK signaling, phosphatidylinositol signaling, and calcium-mediated signaling, predicted from our data, may also play important roles in regulating leaf angle plasticity, which are worthy to be explored in the future.

Because green revolution cereal varieties require a high inorganic fertilizer supply to sustain the maximum yield potential, resulting in serious environmental degradation, the strategy, with enhanced tillering in high-density planting, has been proposed to effectively sustain the high yield of green revolution varieties. Therefore, manipulation of LJ formation and dynamics is a key strategy to increase green revolution yields by controlling population density (Tian et al., 2019; Wang et al., 2020; Wu et al., 2020). In this study, we provided evidence that grain yield in rice with erect leaves generally enhanced by dense planting is primarily due to a smaller reduction in tiller number than that in the wild-type. Although the leaf erectness was proposed to be an important component of ideal plant architecture (Donald, 1968; Khush, 1995; Ort et al., 2015), how erect leaves directly contribute to grain yields per unit area is not yet fully understood. The previous studies reported that erect leaves increase the leaf area index to enhance light capture for photosynthesis and nitrogen use, which could increase crop biomass (Angus et al., 1972; Hikosaka and Hirose, 1997;

Lambert and Johnson, 1978; Sinclair and Sheehy, 1999). Recently, it was found that erect leaves in rice enhance the yield per unit area through dense planting, which resulted from a higher number of panicles per area (Sakamoto et al., 2006). In another study, erect leaves in maize also result in higher yields than normal leaves under dense planting (Tian et al., 2019). However, the grain yield per plant was significantly lower under dense planting compared with normal planting in plants either with erect or normal leaves. Therefore, whether dense planting can increase yields compared with normal planting and/or how erect leaves contribute to higher population yield are still obscure. We analyzed a set of CRISPR lines of key TFs that determine leaf angle via the different cytological regulatory mechanisms in LJs. Under dense planting, the lines with erect leaves not only exhibited increased grain yields compared with the wild-type but also had higher yields under dense planting than both the same lines and wild-type plants under normal planting conditions, primarily due to increased tiller number per unit area (Figures 6B and 6D). Apparently the tillering number per plant was reduced in both wild-type plants and the CRISPR lines under dense planting, but the reduction was more modest in the CRISPR lines versus the wild-type (Figure 6A). Under dense planting, some wheat varieties with erect leaves have more spikes per plant than varieties with normal leaves (Liu et al., 2019). Therefore, it is likely that in both rice and wheat, the tiller number is strongly affected by planting density. Because dense planting might result in shade avoidance syndrome, including a reduced shoot branching (Gonzalez-Grandio et al., 2013), this syndrome would be likely avoided in the varieties with erect leaves under dense planting. The molecular mechanism of how erect leaves affect tillering is an interesting question to be investigated in the future.

Limitations of the Study

As several miRNAs have been reported to play important roles in leaf angle regulation, we performed sRNA-seq and established the global network of miRNAs involved in LJ development and leaf angle formation. Using the psRNATarget online server, we predicted a few miRNA-target pairs including several miRNA-target pairs reported in leaf angle regulation, and most of the predicted miRNA-target pairs that are not reported. It is worthy of further study to reveal whether and/or how these potential miRNA-target pairs regulate LJ development and leaf angle formation.

Resource Availability

Lead Contact

Further information and requests for resources and reagents should be directed to and will be fulfilled by the Lead Contact, Shiyong Sun (sunshiyong@mail.hzau.edu.cn).

Materials Availability

Materials generated in this study are available from the Lead Contact with a completed Materials Transfer Agreement.

Data and Code Availability

The accession number for the datasets in this study is Gene Expression Omnibus (GEO; https://www.ncbi.nlm.nih.gov/geo/): GSE155932.

METHODS

All methods can be found in the accompanying Transparent Methods supplemental file.

SUPPLEMENTAL INFORMATION

Supplemental Information can be found online at https://doi.org/10.1016/j.isci.2020.101489.

ACKNOWLEDGMENTS

We thank Y.D. Zhao for providing the CRISPR/CAS9 vector. This work was supported by funding from the Ministry of Science and Technology of China (grant 2016YFD0100403), The Transgenic Plant Research and Commercialization Project of the Ministry of Agriculture of China (Grant No. 2016ZX08001003-003), the National Natural Science Foundation of China (grant 31671265; 31871227; 31540080), and the National Key Basic Research Foundation of China (2015CB910200).

AUTHOR CONTRIBUTIONS

X.W. and S.S. designed the research; X.W., S.S., R.W., and C.L. analyzed the results and wrote the manuscript; R.W. performed most of the experiments; C.L. and R.W. performed the analysis of transcriptomes; R.W. and Q.L. performed the paraffin sections; R.W. and Z.C. identified the knockout mutants.

DECLARATION OF INTERESTS

The authors declare no competing interests.

Received: May 31, 2020
Revised: August 10, 2020
Accepted: August 18, 2020
Published: September 25, 2020

REFERENCES

Ambavaram, M.M., Krishnan, A., Trijatmiko, K.R., and Pereira, A. (2011). Coordinated activation of cellulose and repression of lignin biosynthesis pathways in rice. Plant Physiol. *155*, 916–931.

Angus, J.F., Jones, R., and Wilso, J.H. (1972). A comparison of barley cultivars with different leaf inclinations. Aust. J. Aguic. Res. *23*, 945–957.

Asahina, M., Tamaki, Y., Sakamoto, T., Shibata, K., Nomura, T., and Yokota, T. (2014). Blue light-promoted rice leaf bending and unrolling are due to up-regulated brassinosteroid biosynthesis genes accompanied by accumulation of castasterone. Phytochemistry *104*, 21–29.

Axtell, M.J. (2013). ShortStack: comprehensive annotation and quantification of small RNA genes. RNA *19*, 740–751.

Bai, M.Y., Zhang, L.Y., Gampala, S.S., Zhu, S.W., Song, W.Y., Chong, K., and Wang, Z.Y. (2007). Functions of OsBZR1 and 14-3-3 proteins in brassinosteroid signaling in rice. Proc. Natl. Acad. Sci. U S A *104*, 13839–13844.

Bao, W.L., O'malley, D.M., Whetten, R., and Sederoff, R.R. (1993). A laccase associated with lignification in loblolly pine xylem. Science *260*, 672–674.

Beighley, D.H. (2010). Growth and production of rice. Soils Plant Growth Crop Prod. *II*, 1–11.

Besseau, S., Hoffmann, L., Geoffroy, P., Lapierre, C., Pollet, B., and Legrand, M. (2007). Flavonoid accumulation in Arabidopsis repressed in lignin synthesis affects auxin transport and plant growth. Plant Cell *19*, 148–162.

Bian, H., Xie, Y., Guo, F., Han, N., Ma, Y., Zeng, Z., Wang, J., Yang, Y., and Zhu, M. (2012). Distinctive expression patterns and roles of the miRNA393/TIR1 homolog module in regulating flag leaf inclination and primary and crown root growth in rice (Oryza sativa). New Phytol. *196*, 149–161.

Chen, R., Shen, L., Wang, D., Wang, F., Zeng, H., Chen, Z., Peng, Y., Lin, Y., Tang, X., Deng, M., et al. (2015). A gene expression profiling of early rice stamen development that reveals inhibition of photosynthetic genes by OsMADS58. Mol. Plant *8*, 1069–1089.

Chen, S., Zhou, L., Xu, P., and Xue, H. (2018). SPOC domain-containing protein Leaf inclination3 interacts with LIP1 to regulate rice leaf inclination through auxin signaling. PLoS Genet. *14*, e1007829.

Dai, M., Hu, Y., Zhao, Y., Liu, H., and Zhou, D. (2007). A WUSCHEL-LIKE HOMEOBOX gene represses a YABBY gene expression required for rice leaf development. Plant Physiol. *144*, 380–390.

Dai, X., and Zhao, P.X. (2011). PsRNATarget: a plant small RNA target analysis server. Nucleic Acids Res. *39*, W155–W159.

del Rió, L.A., Corpas, F.J., Sandalio, L.M., Palma, J.M., Gómez, M., and Barroso, J.B. (2002). Reactive oxygen species, antioxidant systems and nitric oxide in peroxisomes. J. Exp. Bot. *53*, 1255–1272.

Donald, C.M. (1968). The breeding of crop ideotypes. Euphytica *17*, 385–403.

Fornara, F., Pařenicová, L., Falasca, G., Pelucchi, N., Masiero, S., Ciannamea, S., Lopez-Dee, Z., Altamura, M.M., Colombo, L., and Kater, M.M. (2004). Functional characterization of OsMADS18, a member of the AP1/SQUA subfamily of MADS box genes. Plant Physiol. *135*, 2207–2219.

Gao, J., Chen, H., Yang, H., He, Y., Tian, Z., and Li, J. (2018). A brassinosteroid responsive miRNA-target module regulates gibberellin biosynthesis and plant development. New Phytol. *10*, 220.

Gao, Y., and Zhao, Y. (2014). Self-processing of ribozyme-flanked RNAs into guide RNAs in vitro and in vivo for CRISPR-mediated genome editing. J. Integr. Plant Biol. *56*, 343–349.

Gonzalez-Grandio, E., Poza-Carrion, C., Sorzano, C.O., and Cubas, P. (2013). BRANCHED1 promotes axillary bud dormancy in response to shade in Arabidopsis. Plant Cell *25*, 834–850.

Hatsugai, N., Yamada, K., Goto-Yamada, S., and Hara-Nishimura, I. (2015). Vacuolar processing enzyme in plant programmed cell death. Front. Plant Sci. *6*, 234.

Heang, D., and Sassa, H. (2012). Antagonistic actions of HLH/bHLH proteins are involved in grain length and weight in rice. PLoS One *7*, e31325.

Hikosaka, K., and Hirose, T. (1997). Leaf angle as a strategy for light competition: optimal and evolutionarily stable light-extinction coefficient within a leaf canopy. Ecoscience *4*, 501–507.

Hong, Z., Ueguchi-Tanaka, M., Fujioka, S., Takatsuto, S., Yoshida, S., Hasegawa, Y., Ashikari, M., Kitano, H., and Matsuoka, M. (2005). The Rice brassinosteroid-deficient dwarf2 mutant, defective in the rice homolog of Arabidopsis DIMINUTO/DWARF1, is rescued by the endogenously accumulated alternative bioactive brassinosteroid, dolichosterone. Plant Cell *17*, 2243–2254.

Hoshikawa, K. (1989). The Growing Rice Plant: An Anatomical Mono-Graph (Nobunkyo).

Hu, L., Liang, W., Yin, C., Cui, X., Zong, J., Wang, X., Hu, J., and Zhang, D. (2011). Rice MADS3 regulates ROS homeostasis during late anther development. Plant Cell *23*, 515–533.

Ito, M., Sentoku, N., Nishimura, A., Hong, S., Sato, Y., and Matsuoka, M. (2002). Position dependent expression of GL2-type homeobox gene, ROC1: significance for protoderm differentiation and radical pattern formation in early rice embryogenesis. Plant J. *29*, 497–507.

Jiao, Y., Wang, Y., Xue, D., Wang, J., Yan, M., Liu, G., Dong, G., Zeng, D., Lu, Z., Zhu, X., et al. (2010). Regulation of OsSPL14 by OsmiR156 defines ideal plant architecture in rice. Nat. Genet. *42*, 541–544.

Khush, G.S. (1995). Breaking the yield frontier of rice. GeoJournal *35*, 329–332.

Kirik, V., Schrader, A., Uhrig, J.F., and Hulskamp, M. (2007). MIDGET unravels functions of the Arabidopsis topoisomerase VI complex in DNA endoreduplication, chromatin condensation, and transcriptional silencing. Plant Cell *19*, 3100–3110.

Ku, L., Wei, X., Zhang, S., Zhang, J., Guo, S., and Chen, Y. (2011). Cloning and characterization of a putative TAC1 ortholog associated with leaf angle in maize (Zea mays L.). PLoS One *6*, e20621.

Kumagai, E., Hamaoka, N., Araki, T., and Ueno, O. (2014). Dorsoventral asymmetry of photosynthesis and photoinhibition in flag leaves of two rice cultivars that differ in nitrogen response and leaf angle. Physiol. Plant *151*, 533–543.

Lam, E., and Pozo, O. (2000). Caspase-like protease involvement in the control of plant cell death. Plant Mol. Biol. *44*, 417–428.

Lambert, R.J., and Johnson, R.R. (1978). Leaf angle, tassel morphology, and the performance of maize hybrids. Crop Sci. *18*, 499–502.

Lee, J., Park, J.J., Kim, S.L., Yim, J., and An, G. (2007). Mutations in the rice liguleless gene result in a complete loss of the auricle, ligule, and laminar joint. Plant Mol. Biol. *65*, 487–499.

Li, X., Sun, S., Li, C., Qiao, S., Wang, T., Leng, L., Shen, H., and Wang, X. (2014). The Strigolactone-related mutants have enhanced lamina joint inclination phenotype at the seedling stage. J. Genet. Genomics *41*, 605–608.

Liu, H.L., Xu, Y.Y., Xu, Z.H., and Chong, K. (2007). A rice YABBY gene, OsYABBY4, preferentially expresses in developing vascular tissue. Dev. Genes Evol. *217*, 629–637.

Liu, K., Cao, J., Yu, K., Liu, X., Gao, Y., Chen, Q., Zhang, W., Peng, H., Du, J., Xin, M., et al. (2019). Wheat TaSPL8 modulates leaf angle through auxin and brassinosteroid signaling. Plant Physiol. *181*, 179–194.

Liu, X., Yang, C.Y., Miao, R., Zhou, C.L., Cao, P.H., Lan, J., Zhu, X.J., Mou, C.L., Huang, Y.S., Liu, S.J., et al. (2018). DS1/OsEMF1 interacts with OsARF11 to control rice architecture by regulation of brassinosteroid signaling. Rice (N. Y.) *11*, 46.

Lu, C., Jeong, D.H., Kulkarni, K., Pillay, M., Nobuta, K., German, R., Thatcher, S.R., Maher, C., Zhang, L., Ware, D., et al. (2008). Genome-wide analysis for discovery of rice microRNAs reveals natural antisense microRNAs (nat-miRNAs). Proc. Natl. Acad. Sci. U S A *105*, 4951–4956.

Moldenhauer, K., Counce, P., and Hardke, J. (2001). Rice growth and development. In Louisiana Rice Production Handbook, J. Saichuk, ed. (Louisiana State University AgCenter), pp. 9–20, Publ 2321.

Moreno, M.A., Harper, L.C., Krueger, R.W., Dellaporta, S.L., and Freeling, M. (1997). Liguleless1 encodes a nuclear-localized protein required for induction of ligules and auricles during maize leaf organogenesis. Genes Dev. *11*, 616–628.

Ning, J., Zhang, B., Wang, N., Zhou, Y., and Xiong, L. (2011). Increased leaf angle1, a Raf-like MAPKKK that interacts with a nuclear protein family, regulates mechanical tissue formation in the Lamina joint of rice. Plant Cell *23*, 4334–4347.

Ort, D.R., Merchant, S.S., Alric, J., Barkan, A., Blankenship, R.E., Bock, R., Croce, R., Hanson, M.R., Hibberd, J.M., Long, S.P., et al. (2015). Redesigning photosynthesis to sustainably meet global food and bioenergy demand. Proc. Natl. Acad. Sci. U S A *112*, 8529–8536.

Postma-Haarsma, A.D., Rueb, S., Scarpella, E., Besten, W., Hoge, J.H., and Meijer, A.H. (2002). Developmental regulation and downstream effects of the knox class homeobox genes Oskn2 and Oskn3 from rice. Plant Mol. Biol. *48*, 423–441.

Prasad, K., Parameswaran, S., and Vijayraghavan, U. (2005). OsMADS1, a rice MADS-box factor, controls differentiation of specific cell types in the lemma and palea and is an early-acting regulator of inner floral organs. Plant J. *43*, 915–928.

Quiroga, M., Guerrero, C., Botella, M.A., Barceló, A., Amaya, I., Medina, M.I., Alonso, F.J., de Forchetti, S.M., Tigier, H., and Valpuesta, V. (2000). A tomato peroxidase involved in the synthesis of lignin and suberin. Plant Physiol. *112*, 1119–1127.

Ruan, W., Guo, M., Xu, L., Wang, X., Zhao, H., Wang, J., and Yi, K. (2018). An SPX-RLI1 module regulates leaf inclination in response to phosphate availability in rice. Plant Cell *30*, 853–870.

Sakamoto, T., Morinaka, Y., Ohnishi, T., Sunohara, H., Fujioka, S., Ueguchi-Tanaka, M., Mizutani, M., Sakata, K., Takatsuto, S., Yoshida, S., et al. (2006). Erect leaves caused by brassinosteroid deficiency increase biomass production and grain yield in rice. Nat. Biotechnol. *24*, 105–109.

Sang, X.C., Li, Y.F., Luo, Z.K., Ren, D.Y., Fang, L.K., Wang, N., Zhao, F.M., Ling, Y.H., Yang, Z.L., Liu, Y.S., et al. (2012). CHIMERIC FLORAL ORGANS1, encoding a monocot-specific MADS box protein, regulates floral organ identity in rice. Plant Physiol. *160*, 788–807.

Shimada, A., Ueguchi-Tanaka, M., Sakamoto, T., Fujioka, S., Takatsuto, S., Yoshida, S., Sazuka, T., Ashikari, M., and Matsuoka, M. (2006). The rice SPINDLY gene functions as a negative regulator of gibberellin signaling by controlling the suppressive function of the DELLA protein, SLR1, and modulating brassinosteroid synthesis. Plant J. *48*, 390–402.

Sinclair, T.R., and Sheehy, J.E. (1999). Erect leaves and photosynthesis in rice. Science *283*, 1455.

Sun, S., Chen, D., Li, X., Qiao, S., Shi, C., Li, C., Shen, H., and Wang, X. (2015). Brassinosteroid signaling regulates leaf erectness in Oryza sativa via the control of a specific U-type cyclin and cell proliferation. Dev. Cell *34*, 220–228.

Tanaka, A., Nakagawa, H., Tomita, C., Shimatani, Z., Ohtake, M., Nomura, T., Jiang, C.J., Dubouzet, J.G., Kikuchi, S., Sekimoto, H., et al. (2009). BRASSINOSTEROID UPREGULATED1, encoding a helix-loop-helix protein, is a novel gene involved in brassinosteroid signaling and controls bending of the lamina joint in rice. Plant Physiol. *151*, 669–680.

Tian, J., Wang, C., Xia, J., Wu, L., Xu, G., Wu, W., Li, D., Qin, W., Han, X., Chen, Q., et al. (2019). Teosinte ligule allele narrows plant architecture and enhances high-density maize yields. Science *365*, 658–664.

Tsuda, K., Kurata, N., Ohyanagi, H., and Hake, S. (2014). Genome-wide study of KNOX regulatory network reveals brassinosteroid catabolic genes important for shoot meristem function in rice. Plant Cell *26*, 3488–3500.

Tzin, V., and Galili, G. (2010). New insights into the shikimate and aromatic amino acids biosynthesis pathways in plants. Mol. Plant *3*, 956–972.

Vogt, T. (2010). Phenylpropanoid biosynthesis. Mol. Plant *3*, 2–20.

Walsh, J., Waters, C.A., and Freeling, M. (1997). The maize gene liguleless2 encodes a basic leucine zipper protein involved in the establishment of the leaf blade-sheath boundary. Genes Dev. *11*, 208–218.

Wang, L., Xu, Y., Zhang, C., Ma, Q., Joo, S.H., Kim, S.K., Xu, Z.H., and Chong, K. (2008). OsLIC, a novel CCCH-type zinc finger protein with transcription activation, mediates rice architecture via brassinosteroids signaling. PLoS One *3*, e3521.

Wang, S.T., Sun, X.L., Hoshino, Y., Yu, Y., Jia, B., Sun, Z.W., Sun, M.Z., Duan, X.B., and Zhu, Y.M. (2014). MicroRNA319 positively regulates cold tolerance by targeting OsPCF6 and OsTCP21 in rice (oryza sativa L.). PLoS One *9*, 1–12.

Wang, Y.X., Shang, L.G., Yu, H., Zeng, L.J., Hu, J., Ni, S., Rao, Y.C., Li, S.F., Chu, J.F., Meng, X.B., et al. (2020). A strigolactones biosynthesis gene contributed to the Green Revolution in rice. Mol. Plant *13*, 923–932.

Wu, K., Wang, S.S., Song, W.Z., Zhang, J.Q., Wang, Y., Liu, Q., Yu, J.P., Ye, Y.F., Li, S., Chen, J.F., et al. (2020). Enhanced sustainable green revolution yield via nitrogen-responsive chromatin modulation in rice. Science *367*, eaaz2046.

Wu, X., Tang, D., Li, M., Wang, K., and Cheng, Z. (2013). Loose Plant Architecture1, an INDETERMINATE DOMAIN protein involved in shoot gravitropism, regulates plant architecture in rice. Plant Physiol. *161*, 317–329.

Yamamuro, C., Ihara, Y., Wu, X., Noguchi, T., Fujioka, S., Takatsuto, S., Ashikari, M., Kitano, H., and Matsuoka, M. (2000). Loss of function of a rice brassinosteroid insensitive1 homolog prevents internode elongation and bending of the lamina joint. Plant Cell *12*, 1591–1606.

Yu, C.P., Chen, S.C., Chang, Y.M., Liu, W.Y., Lin, H.H., Lin, J.J., Chen, H.J., Lu, Y.J., Wu, Y.H., Lu, M.Y., et al. (2015). Transcriptome dynamics of developing maize leaves and genomewide prediction of cis elements and their cognate transcription factors. Proc. Natl. Acad. Sci. U S A *112*, E2477–E2486.

Yuan, J., Yan, R., Krämer, A., Eckerdt, F., Roller, M., Kaufmann, M., and Strebhardt, K. (2004). Cyclin B1 depletion inhibits proliferation and induces apoptosis in human tumor cells. Oncogene *23*, 5843–5852.

Zhan, J.P., Thakare, D., Ma, C., Lloyd, A., Nixon, N.M., Arakaki, A.M., Burnett, W.J., Logan, K.O., Wang, D.F., Wang, X.F., et al. (2015). RNA sequencing of laser-capture microdissected compartments of the maize kernel identifies regulatory modules associated with endosperm cell differentiation. Plant Cell *27*, 513–531.

Zhang, C., Bai, M.Y., and Chong, K. (2014). Brassinosteroid-mediated regulation of agronomic traits in rice. Plant Cell Rep. *33*, 683–696.

Zhang, L.Y., Bai, M.Y., Wu, J., Zhu, J.Y., Wang, H., Zhang, Z., Wang, W., Sun, Y., Zhao, J., Sun, X.,

et al. (2009). Antagonistic HLH/bHLH transcription factors mediate brassinosteroid regulation of cell elongation and plant development in rice and Arabidopsis. Plant Cell *21*, 3767–3780.

Zhang, S., Wang, S., Xu, Y., Yu, C., Shen, C., Qian, Q., Geisler, M., Jiang de, A., and Qi, Y. (2015). The auxin response factor, OsARF19, controls rice leaf angles through positively regulating OsGH3-5 and OsBRI1. Plant Cell Environ. *38*, 638–654.

Zhang, Y.C., Yu, Y., Wang, C.Y., Li, Z.Y., Liu, Q., Xu, J., Liao, J.Y., Wang, X.J., Qu, L.H., Chen, F., et al. (2013). Overexpression of microRNA OsmiR397 improves rice yield by increasing grain size and promoting panicle branching. Nat. Biotechnol. *31*, 848–852.

Zhao, S.Q., Hu, J., Guo, L.B., Qian, Q., and Xue, H.W. (2010). Rice leaf inclination2, a VIN3-like protein, regulates leaf angle through modulating cell division of the collar. Cell Res. *20*, 935–947.

Zhao, S.Q., Xiang, J.J., and Xue, H.W. (2013). Studies on the rice LEAF INCLINATION1 (LC1), an IAA–amido synthetase, reveal the effects of auxin in leaf inclination control. Mol. Plant *6*, 174–187.

Zhou, L.J., Xiao, L.T., and Xue, H.W. (2017). Dynamic cytology and transcriptional regulation of rice lamina joint development. Plant Physiol. *174*, 1728–1746.

Zhou, X.Y., Jenks, M.A., Liu, J., Liu, A.L., Zhang, X.W., Xiang, J.H., Zou, J., Peng, Y., and Chen, X.B. (2013). Overexpression of transcription factor OsWR2 regulates wax and cutin biosynthesis in rice and enhances its tolerance to water deficit. Plant Mol. Biol. *32*, 719–731.

Zhu, J.Q., van der Werf, W., Anten, N.R., Vos, J., and Evers, J.B. (2015). The contribution of phenotypic plasticity to complementary light capture in plant mixtures. New Phytol. *207*, 1213–1222.

iScience, Volume *23*

Supplemental Information

Spatiotemporal Resolved Leaf Angle Establishment Improves Rice Grain Yield via Controlling Population Density

Rongna Wang, Chang Liu, Qinzhong Li, Zhina Chen, Shiyong Sun, and Xuelu Wang

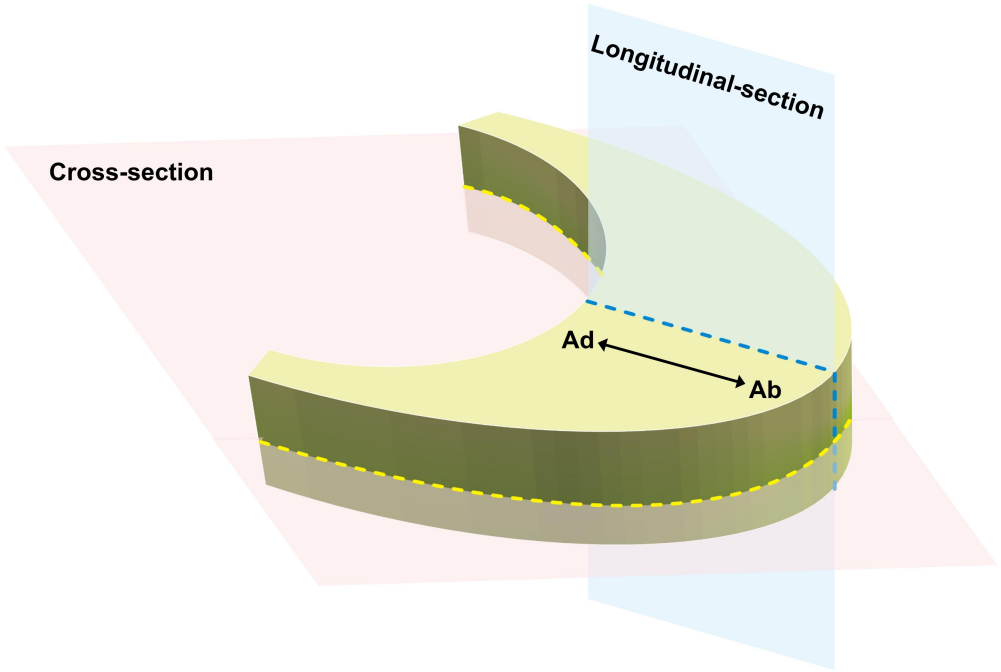

Figure S1. 3D schematics diagram of the positions of the paraffin sections produced from rice LJs, Related to Figure 1.

The cross section is indicated in pink, and the longitudinal-section is indicated in blue. Ad and Ab represent the adaxial and abaxial sides of the LJ, respectively.

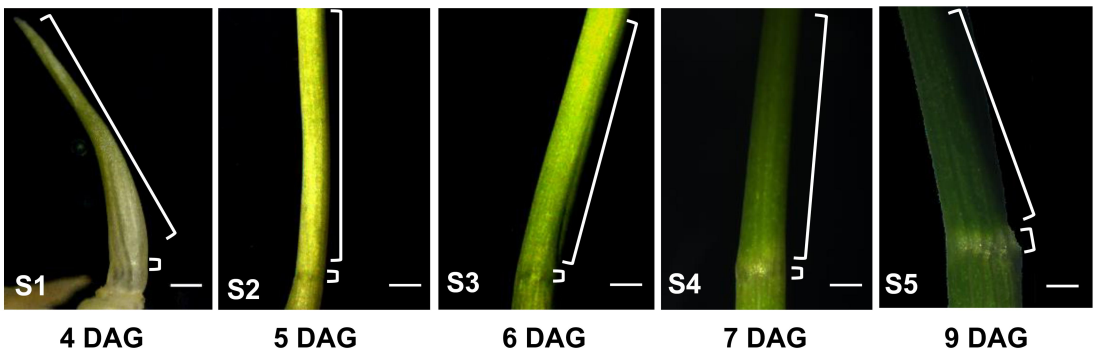

Figure S2. The regions of the first complete leaf collected for RNA-seq analysis at five stages of development, Related to Figure 2 and Figure 3.

The blade regions used for RNA-seq analysis are adjacent to LJs; the LJ regions include the LJs. DAG, days after germination. Scale bars, 500 μm.

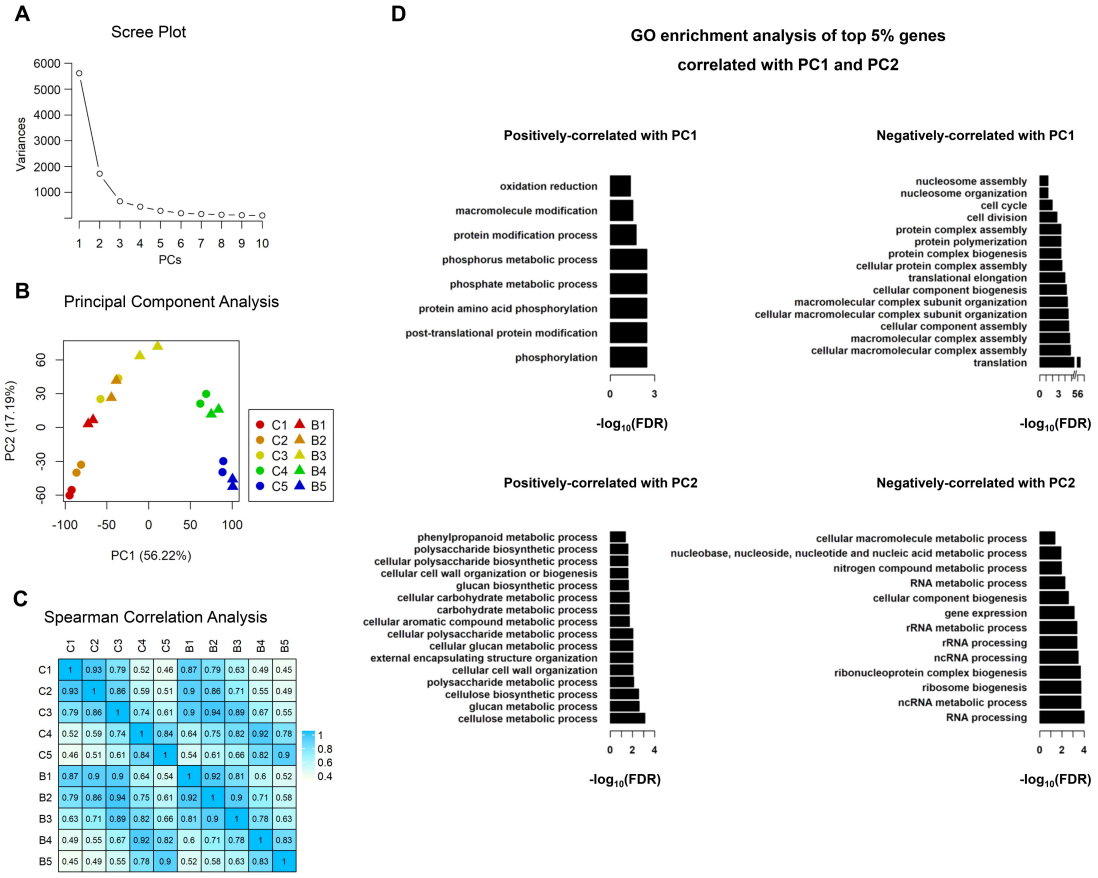

Figure S3. Correlation among the different samples and replicates used for mRNA sequencing, Related to Figure 2.

A, Scree plot for PCA.

B, Principal component analysis (PCA) of 20 libraries from LJs and blades at five stages of development (2 biological replicates per sample). The biological replicates are indicated by the same color and shape; circle represents the LJ, triangle represents the blade; C1 to C5 indicate LJ samples at five stages of development, B1 to B5 indicate blade samples at five stages of development. The proportions of variance represented by PC1 and PC2 are indicated in brackets.

C, GO enrichment analysis (FDR ≤ 0.05) of the top 5% of genes positively or negatively correlated to PC1 and PC2.

D, Spearman's correlation coefficients (SCCs) analysis of the transcriptomes from ten samples using the transformed value $\log_2$(FPKM+1) of genes with more than 1 FPKM in at least one sample.

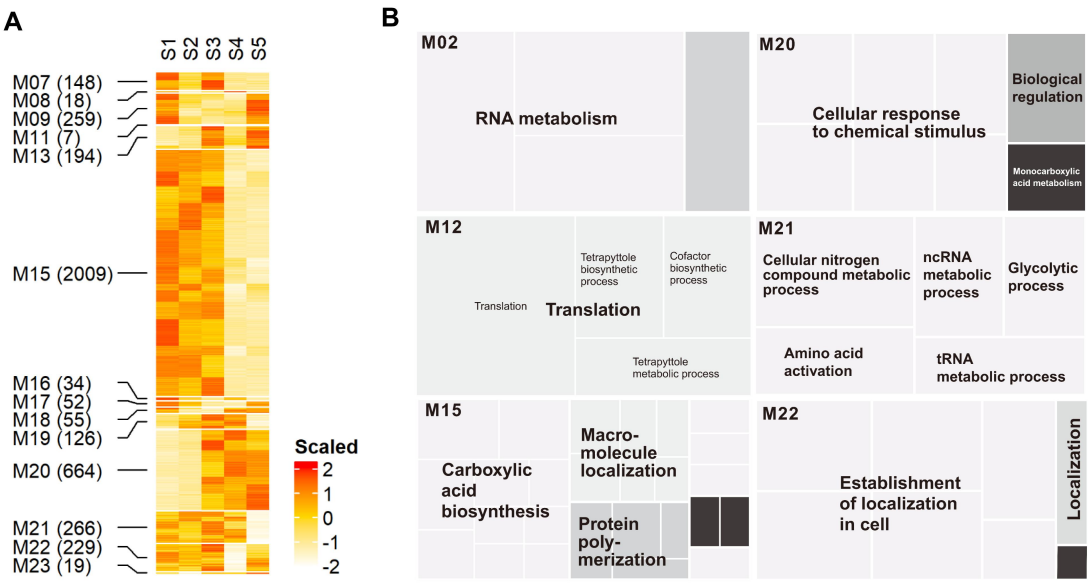

Figure S4. The remained clusters of DEGs and the GO enrichment analysis, Related to Figure 2.

A, Remained clusters of DEGs in LJs. The expression values were normalized using the Z-score method; the number of genes in each cluster is indicated in brackets.

B, Biological processes revealed by GO enrichment analysis (FDR ≤ 0.05) in the remained clusters. The related GO terms are displayed in similar colors; aggregate size indicates the significance of the GO term.

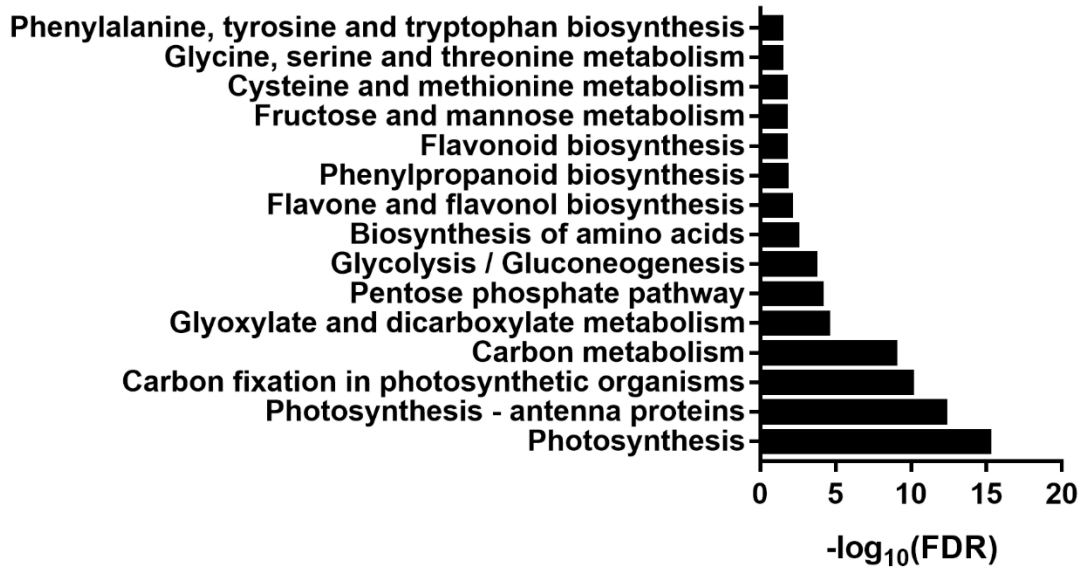

Figure S5. Enriched functional processes in cluster M04 determined by KEGG pathway analysis (FDR ≤ 0.05) , Related to Figure 2.

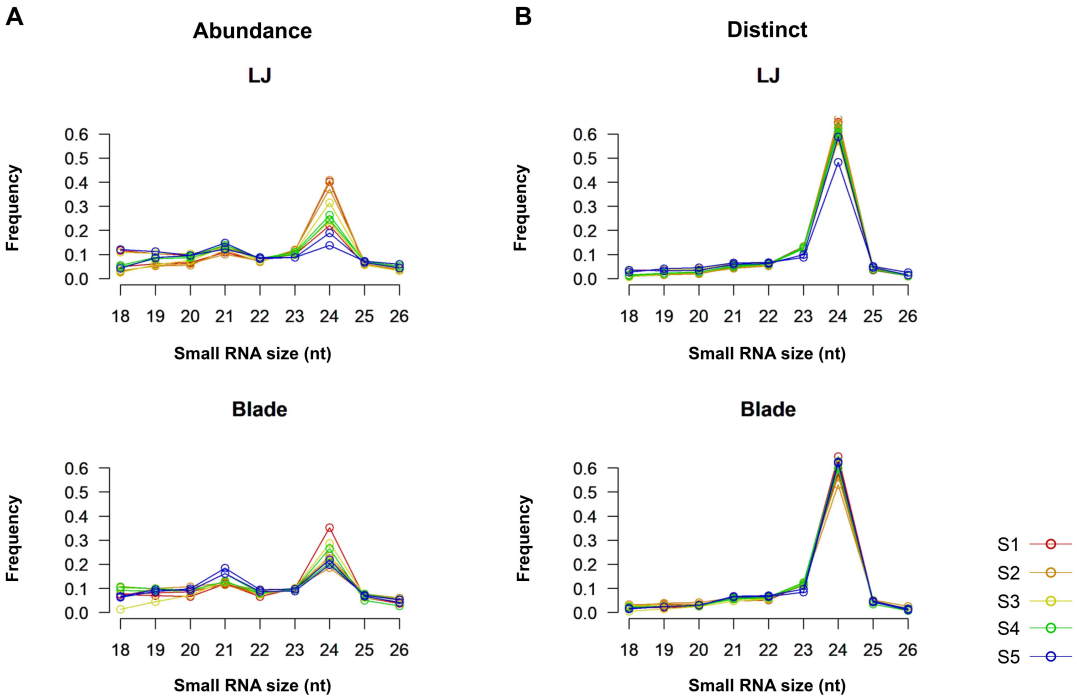

Figure S6. Size distribution of small RNAs in libraries from LJs and blades at five stages of development, Related to Figure 3.

The sizes of small RNAs are plotted versus frequency (percentage) among total sequences (A) and distinct sequences (B). The distinct sequences represent the small RNA species in each library after removing the duplicates from total sequences.

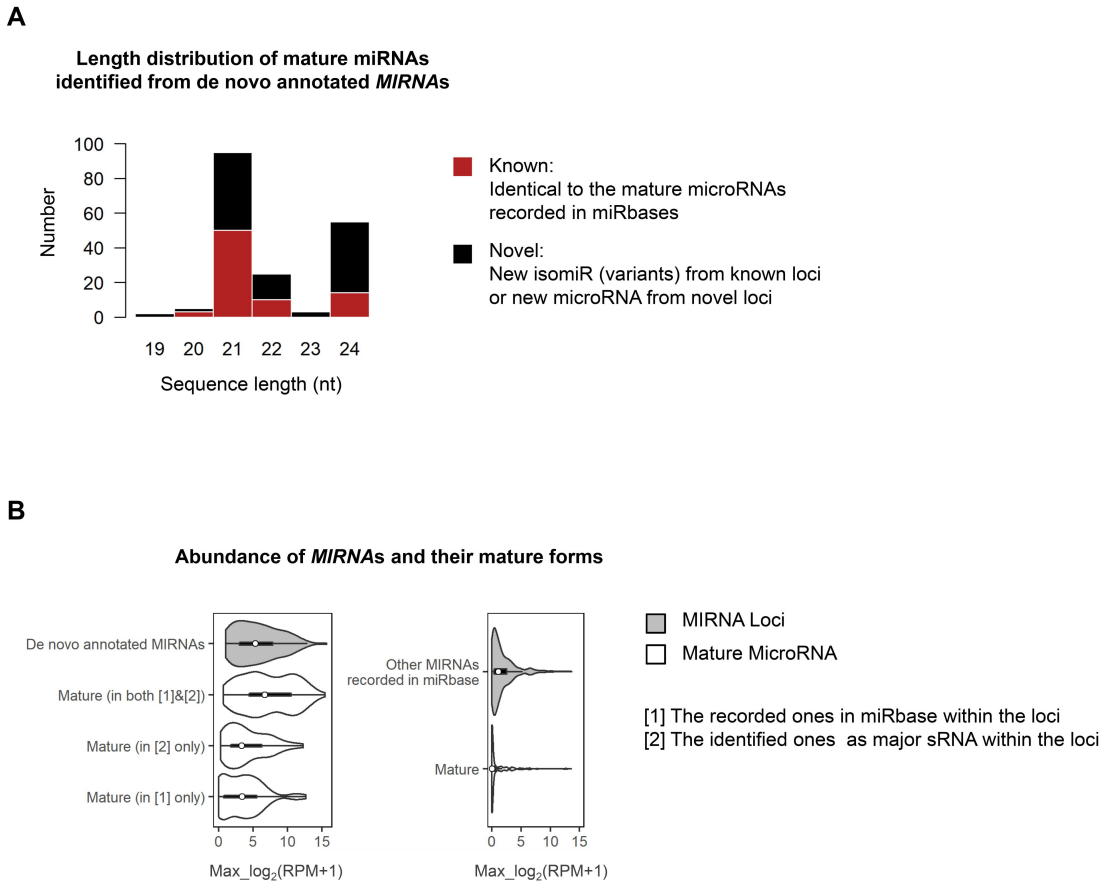

Figure S7. Characters and abundance of mature miRNAs, Related to Figure 3.
A, Characters of the mature miRNAs identified from de novo annotated *MIRNAs*.
B, Abundance of *MIRNAs* and their mature miRNAs identified by de novo annotation and miRBase.

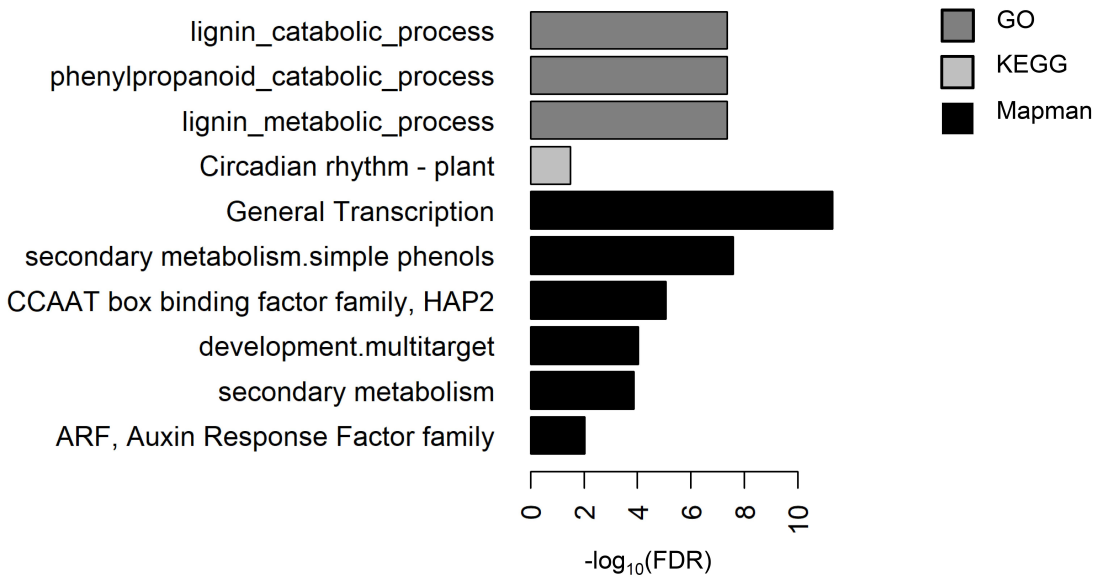

Figure S8. Enriched functional processes (GO/KEGG/MAPMAN; FDR ≤ 0.05) for predicted target genes by stage-specific miRNAs that are differentially expressed in LJs during development (expectation ≤ 2.5), Related to Figure 3.

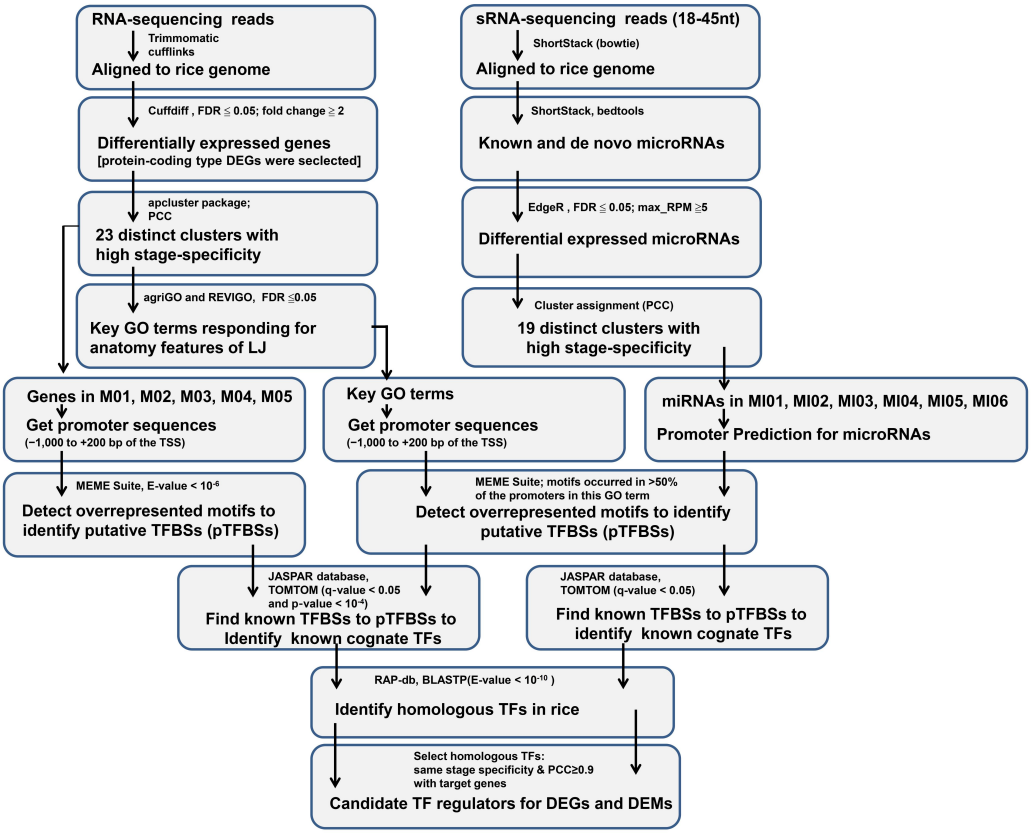

Figure S9. The detailed pipeline used to predict TFBSs and candidate TFs for LJ development in rice, Related to Figure 4.

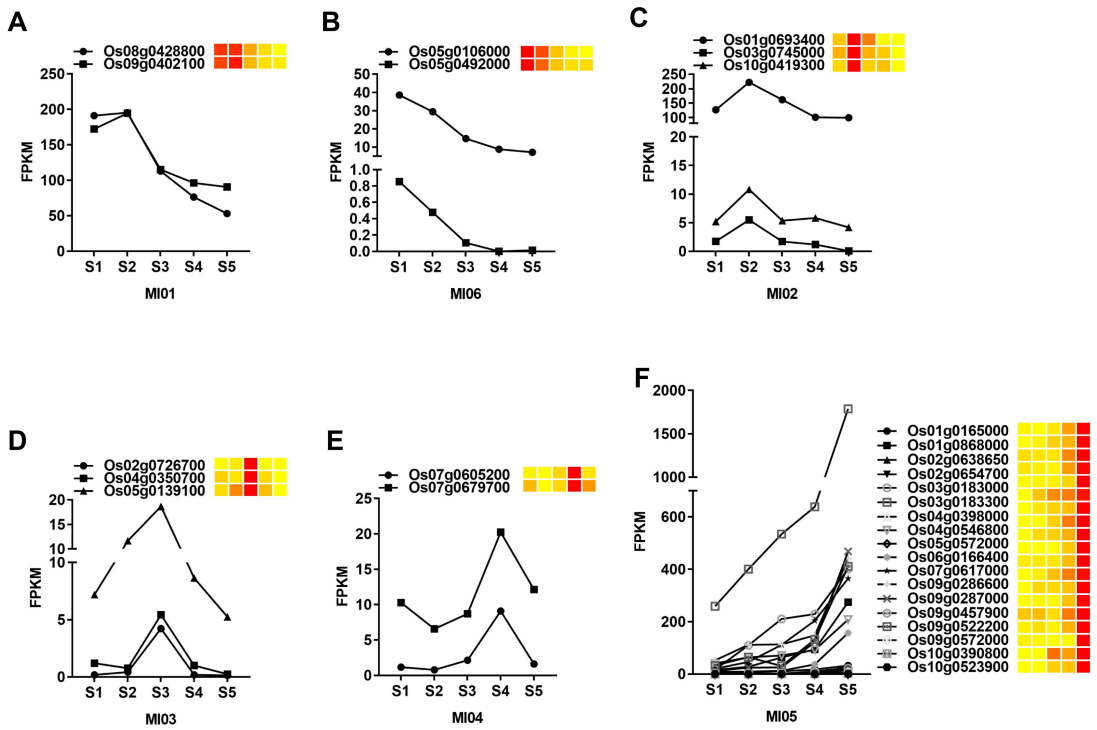

Figure S10. Identification of key TFs determining the expression patterns of *MIRNAs* in LJs, Related to Figure 4.

The FPKM values and the normalized expression values at five stages of development are shown. Heatmaps represent the normalized expression values determined using the Z-score method.

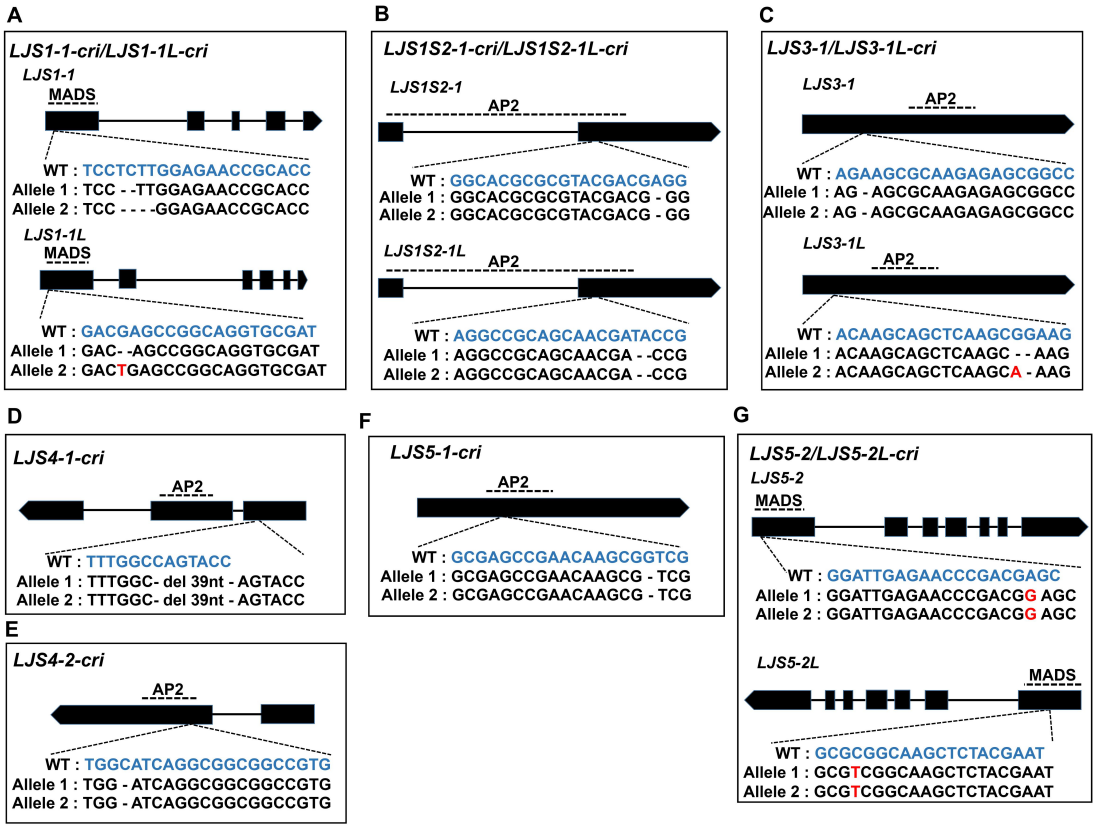

Figure S11. Sequencing results for the knockout lines of the candidate TFs generated by CRISPR/Cas9, Related to Figure 4.

The gRNA-targeting sites are indicated in blue. Insertions are highlighted in red and deletions are indicated by dashes.

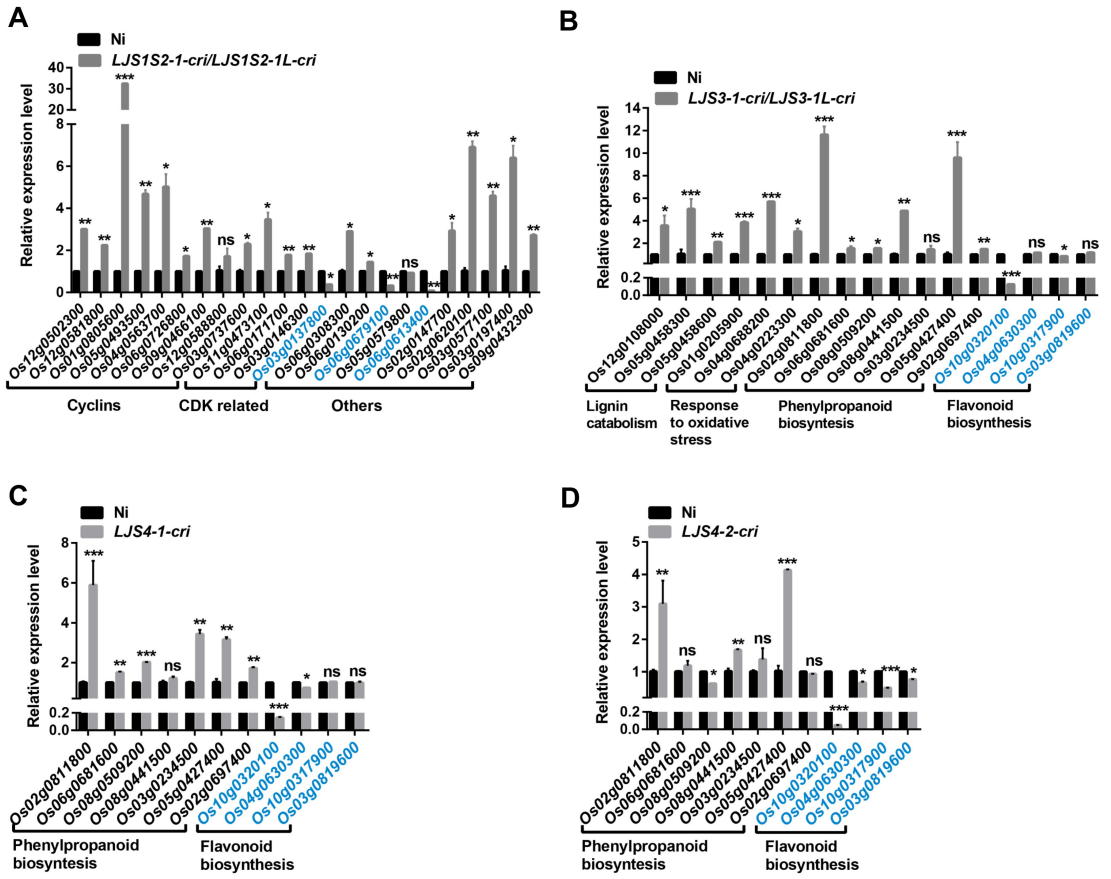

Figure S12. Relative expression levels of putative target genes in specific GO terms, Related to Figure 5.

A, Relative expression levels of putative target genes from the cell cycle term in M06, which were detected in the LJs of *LJS1S2-1-cri/LJS1S2-1L-cri* and Ni at S1, respectively. Gene IDs in black represent genes with positive roles in the cell cycle, whereas gene IDs in blue represent genes with negative roles in the cell cycle.

B, Relative expression levels of putative target genes in the GO terms lignin catabolism and response to oxidative stress in M03, and phenylpropanoid biosynthesis and flavonoid biosynthesis in M04, which were detected in the LJs of *LJS3-1-cri*/*LJS3-1L-cri* and wild-type Ni. Gene IDs in black represent genes with positive roles in lignin biosynthesis, whereas gene IDs in blue represent genes with negative roles in lignin biosynthesis.

C,**D**, Relative expression levels of putative target genes in the GO terms phenylpropanoid biosynthesis and flavonoid biosynthesis in M04, which werre detected in the LJs of *LJS4-1-cri*, *LJS4-2-cri*, and wild-type Ni at S4. Gene IDs in black represent genes with positive roles in lignin biosynthesis, whereas gene IDs in blue represent genes with negative roles in lignin biosynthesis.

The expression levels in Ni were defined as 1. Data are means ± SD. n=3. Significance was tested using Student's *t*-test with $*p < 0.05$, $**p < 0.01$, $***p < 0.001$, and ns indicates no significance.

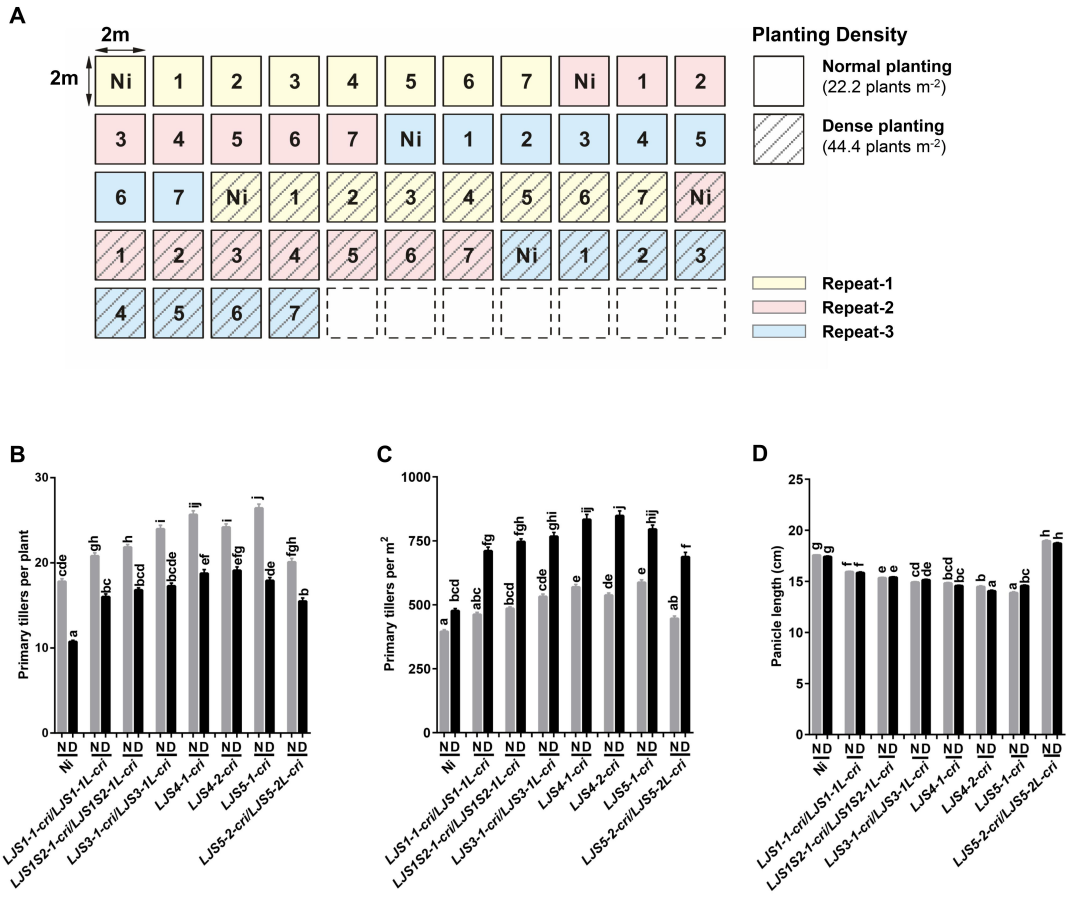

Figure S13. Tiller number and panicle length under the different planting densities, Related to Figure 6.

A, Sketch map of the paddy trial in Wuhan, China in 2019 used to compared knockout lines with erect leaves and wild-type plants (Ni) under two planting densities with three replicates. Knockout lines 1-7 are 1-*LJS1-1cri/LJS1-1L-cri*, 2-*LJS1S2-1-cri/LJS1S2-1L-cri*, 3-*LJS3-1-cri/LJS3-1L-cri*, 4-*LJS4-1-cri*, 5-*LJS4-2-cri*, 6-*LJS5-1-cri*, and 7-*LJS5-2-cri/LJS5-2L-cri*.

B, Primary tiller number per plant under different planting densities. n = 40.

C, Primary tiller number per square meter under different planting densities.

D, Panicle length under different planting densities. n = 70.

N: normal planting (22.2 plants m^{-2}); D: dense planting (44.4 plants m^{-2}). Data are the means ± SE. Lowercase letters indicate significant differences at the level of $P < 0.05$ within a parameter (Tukey's Honest Significant Difference test).

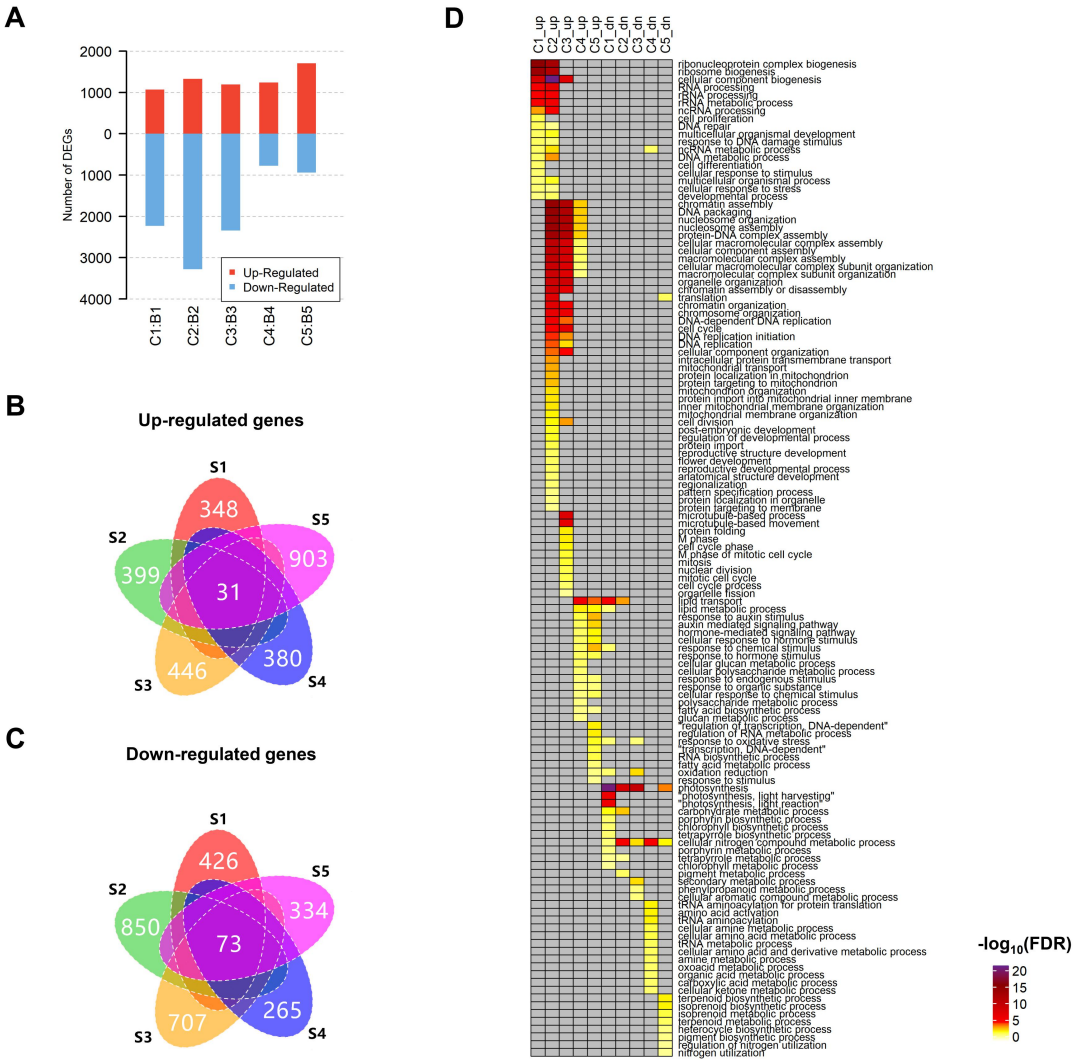

Figure S14. Identification of genes with organ-specificity at five stages of development, Related to Figure 2.

A, Number of organ-specific genes at each stage (FDR ≤ 0.05 and fold change ≥ 2).

B, Up-regulated genes in LJs compared to blades at each stage.

C, Down-regulated genes in LJs compared to blades at each stage.

D, Enriched GO terms in the biological processes category (FDR ≤ 0.05) for the organ-specific genes at each stage. Gray box indicates that a GO term is not enriched in a specific gene set.

Transparent Methods

Plant growth conditions and sample collection

The rice variety used in this study was *japonica* (*Oryza sativa*) cultivar, Nipponbare (Ni). The seeds were soaked in distilled water at room temperature for 1 day and imbibed for 2 days in water at 37°C in a constant temperature incubator (referred to as the first and second day after germination, respectively). The water was changed twice daily. The germinated seeds were transferred to 96-well plates with cut bottoms and grown in water under a 16 h (light, 28°C)/8 h (dark, 25°C) cycle. LJ and blade tissue form the first complete leaves of seedlings were separately cut and collected on the 4^{th}, 5^{th}, 6^{th}, 7^{th}, and 9^{th} day after germination, the length of LJ were less than 1 mm, and the length of blade was less than 10 mm. In addition, the leaf materials inside the outer leaf were removed respectively. Approximately 150 seedlings at each stage were dissected to isolate RNA for LJs and leaf blades. The collected tissues were immediately frozen in liquid nitrogen and subjected to total RNA extraction with TRIzol (Invitrogen). Two biological replicates per sample were produced to construct RNA-seq and small RNA-seq libraries.

Paraffin sectioning

LJ and blade tissues were fixed in FAA solution (50% ethanol, 5% acetic acid, and 10% formaldehyde in water), vacuum infiltrated for one hour, dehydrated with a graded ethanol series (from 50% ethanol to absolute ethanol), and embedded in paraffin. Microtome sections (7 um) were cut with a paraffin-slicing machine (Leica) and affixed to egg white-glycerin-coated slides. The sections were de-paraffinized in xylene, dehydrated through a graded ethanol series, and stained with Safranin O/Fast Green, and observed under a light microscope (Zeiss, Germany).

RNA library preparation, sequencing, and data processing

RNA-seq libraries were constructed using a NEBNext® Ultra™ RNA Library Prep Kit for Illumina® (NEB, USA) and sequenced on the Illumina HiSeq 4000 platform to generate 150 bp paired-end reads. After removing low-quality reads, the clean reads

were trimmed with Trimmomatic-0.36 and then mapped to the rice reference genome rice IRGSP-1.0 with TopHat v2.1.1 (Kim et al., 2013). The uniquely mapped reads were used to calculate FPKM (fragments per kilobase of transcript per million reads) values for the genes with Cufflinks v2.2.1 (Trapnell et al., 2012) to estimate their expression levels in different samples. The rice genome and gene annotation file was downloaded from Ensembl Plants (http://plants.ensembl.org/index.html). Principal component analysis (PCA) and Spearman's correlation coefficients (SCCs) analysis based on gene expression profiles were performed using the prcomp and cor functions in R software.

Identification of DEGs and DEMs, clustering, and functional enrichment analysis

Differentially expressed genes (DEGs) in each pair of samples were identified using Cuffdiff (Cufflinks v2.2.1, FDR ≤ 0.05 and Fold change ≥ 2) and merged into three gene sets based on stage-level differences between LJ samples only or blade samples only and the organ-level differences between LJs and blades at the same stage. The stage-level DEGs for LJs or blades with annotated coding sequences were used to perform clustering to obtain predominant gene sets with distinct stage specificity to uncover active functional modules during organ development in subsequent analysis. The DEGs were assigned into small clusters by the affinity propagation-clustering algorithm (Bodenhofer et al., 2011) using the R package apcluster with default parameters. Given that many of these clusters still exhibited similar stage specificity, we further combined them into 23 gene sets based on their similarity to the expected expression pattern with the highest Pearson correlation coefficient in 5 LJ samples (PCC5). The expected patterns were determined by permuting five elements with values of “1” or “0” in a numeric array, which represent single stage or stages-group specificity. The DEGs between LJs and blades at each stage were defined as organ-specific genes.

The differentially expressed microRNAs (DEMs) for each sample pair were identified with edgeR (FDR ≤ 0.05; maximum expression value ≥ 5RPM). The DEMs between LJ samples were directly clustered into 19 stage-specific modules, based on their similarity to the expected expression pattern with the highest PCC, as mentioned

above.

Gene ontology (GO) enrichment analysis (FDR ≤ 0.05) of particular gene sets was performed using the web tool agriGO (http://bioinfo.cau.edu.cn/agriGO/index.php), and the GO terms were summarized with REVIGO (Supek et al., 2011). The KEGG enrichment analysis (FDR ≤ 0.05) for particular gene sets was performed with the R package "clusterProfiler", and the pathway annotations of rice genes were downloaded from KEGG (https://www.genome.jp/kegg/).

Small RNA library preparation, sequencing, and miRNA identification

The total RNAs were sent to BGI (Shenzhen, China) for small RNA library construction and high-throughput sequencing on the BGISEQ-500 platform. Adaptor sequences, contamination, and low-quality reads were removed from the raw reads. Mapping of the clean data to the reference genome and de novo *MIRNA* identification were performed with ShortStack (v 3.8.2; parameter set: --dicermin 18 --dicermax 26 --foldsize 400) for each sample and merged *MIRNA* loci were obtained with bedtools v2.17.0. The identified *MIRNA*s (microRNA loci) were compared to the annotated *MIRNA*s in miRBase (v21; osa.gff3). The major sRNA species with the highest abundance identified from each *MIRNA* locus were considered to be the mature miRNAs in different samples, which were also compared with he mature miRNAs in miRBase. A locus with a mature miRNA whose sequence was similar to that of a known miRNA annotated in miRBase was considered to be a paralogous member of that known family (Meyers et al., 2008). A mature miRNA whose sequence differed from the known sequence at the same locus was considered to be a variant or isomiR.

Target prediction and differentially expressed miRNAs

Target prediction of the mature miRNAs was performed with psRNATarget (http://plantgrn.noble.org/psRNATarget/; expectation ≤ 2.5), and differentially expressed miRNAs between samples were detected with edgeR (FDR ≤ 0.05; maximum RPM ≥ 5). The miRNAs identified in comparisons between C1-C5 were considered to be stage-specific miRNAs that function in LJ development. The stage-specific miRNAs were directly assigned to 19 clusters based on their expression dynamics with the highest similarity to the expected expression patterns, which

represent single stage or stages-group specific miRNAs, as mentioned above.

Identification of cis-motifs and candidate cognate TFs

For identification of cis-elements, first, the gene sets including all the genes in clusters M01 to M05 were used. Second, we also used genes sets enriched in GO terms which were the main developmental features of LJ in different stages, including lignin catabolism, lipid metabolism, lipid transport, response to oxidative stress in M03, carbohydrate catabolism in M04, and the cell cycle in M06. To predict TFs which potentially regulated specific gene sets, first, the overrepresented motifs in promoters of genes in the specific gene set were detected using the MEME program (Bailey and Elkan, 1994): for predicting motifs in gene sets M01-M05, the top 10 motifs with E-value $\leq 10^{-6}$ were selected as putative transcription factor binding sites (pTFBSs); for predicting motifs in gene sets of GO terms, the top 10 motifs that occurred in $\geq$ 50% of the promoters were selected as pTFBSs. Then, the pTFBSs were compared to known cis-motifs (JASPAR CORE database) using the TOMTOM program (Gupta et al., 2007) to identify the significantly similar binding sites (q-value $\leq$ 0.05 and p-value $\leq 10^{-4}$) that could be recognized by known cognate TFs. Third, the rice homologs of these cognate TFs were identified by BLASTp analysis (e-value $\leq 10^{-10}$; the protein sequences of cognate TFs and rice homologs are downloaded from UniProt and RAP-DB, respectively). Finally, the candidate TFs were identified with two characters: first, they belonged to the same TF family with the cognate TFs, which is predicted by plantTFDB (Jin et al., 2017; http://planttfdb.cbi.pku.edu.cn/); second, they exhibited the similar stage specificity with their predicted targets (PCC5 $\geq$ 0.9). Notably, the TF-targeted genes are the genes from the corresponding gene set whose promoters contain the TF-specific pTFBS from above MEME analysis. We have showed the detailed pipeline in Supplementary Figure 9.

The identified *MIRNA*s (microRNA loci) were compared with the annotations of protein-coding genes (https://rapdb.dna.affrc.go.jp/) to uncover intragenic and intergenic *MIRNA*s (Cui et al., 2009). Given that the intragenic *MIRNA*s were potentially transcribed as a part of their overlapping genes (Lee et al., 2004), their promoter regions were considered to be the same as those of these overlapping genes. To predict the promoters of intergenic *MIRNA*s, the specified upstream regions were

extracted as previously described, which were considered to include TSSs driving transcription (Bailey and Elkan, 1994). The method used to predict TFs regulating miRNA expression was almost the same as that used to predict the regulators of genes from the enriched GO terms mentioned above, except that a threshold of q-value ≤ 0.05 was used (TOMTOM) in the pTFBS comparisons to retain enough results for the clusters we were interested in.

Vector construction and plant transformation

To generate the CRISPR/Cas9 knockout mutants, the pCXUN-CAS9 vector (He et al., 2017) was used. The CRISPR target sequences for selected TF genes were obtained from CRISPR-P 2.0 (http://crispr.hzau.edu.cn/CRISPR2/). To genotype homozygous mutants generated by CRISPR/Cas9, less than 800 bp DNA fragments covering the CRISPR target sequences were amplified and sequenced.

RNA extraction and RT-qPCR

Total RNA was extracted from the samples using the TRIzol method (DP432, Tiangen). First-strand cDNA was synthesized using a PrimeScript RT reagent kit (TaKaRa). For RT-qPCR, SYBRMaster Mix for PCR (Invitrogen) was used. *OsUBQ* (*Os03g0234200*) was used as an internal control to normalize the data. Three biological repeats were performed. The primers are listed in Table S7.

Paddy trials and yield evaluation under different planting densities

Paddy trials were conducted in Wuhan in 2019. The KO and wild-type rice plants were grown in a paddy field with row spacing and plant spacing in a row at a distance of 30 × 15 cm (22.2 plants per m^2) or 15 × 15 cm (44.4 plants per m^2). Each treatment was replicated three times in randomized blocks. Each plot was 2 × 2 m. The number of tillers per treatment was counted in the field from 20 plants excluding marginal plants. Fifty plants were harvested from each plot excluding marginal plants. Tillers with fertile panicles (more than 5 fertile seeds) and panicle length were determined from approximately 30 plants. After harvest, the plants were dried for 7 days, and 1,000- grain weight and grain yield per plant were measured from approximately 30 plants. Grain yield was converted to value per hectare. Standard statistical procedures

were used to analyze the data using SPSS 17.0 (Softonic International, Barcelona, Spain). Tukey's Honest Significant Difference test was used for multiple comparisons at the $P < 0.05$ level.

Supplemental References

Bailey, T.L. and Elkan, C. (1994). Fitting a mixture model by expectation maximization to discover motifs in biopolymers. Proc. Int. Conf. Intell. Syst. Mol. Biol. *2*, 28-36.

Bodenhofer, U., Kothmeier, A., and Hochreiter, S. (2011). APCluster: an R package for affinity propagation clustering. Bioinformatics *27*, 2463-2464.

Cui, X., Xu, S., Mu, D., and Yang, Z. (2009). Genomic analysis of rice microRNA promoters and clusters. Gene *431*, 61-66.

Gupta, S., Stamatoyannopoulos, J. A., Bailey, T. L., and Noble, W. S. Quantifying similarity between motifs. Genome Biol. *8*, R14 (2007).

He, Y., Zhang, T., Yang, N., Xu, M., Yan, L., Wang. L., Wang, R., and Zhao, Y. (2017). Self-cleaving ribozymes enable the production of guide RNAs from unlimited choices of promoters for CRISPR/Cas9 mediated genome editing. J. Genet. Genomics *44*, 469-472.

Jin, J., Tian, F., Yang, D., Meng, Y., Kong, L., Luo, J., and Gao, G. (2017). PlantTFDB 4.0: toward a central hub for transcription factors and regulatory interactions in plants. Nucleic Acids Res. *45*, D1040-D1045.

Kim, D., Pertea, G., Trapnell, C., Pimentel, H., Kelley, R., and Salzberg, S.L. (2013). TopHat2: accurate alignment of transcriptomes in the presence of insertions, deletions and gene fusions. Genome Biol. *14*, R36.

Lee, Y., Kim, M., Han, J., Yeom, K., Lee, S., Baek, S.H., and Kim, V.N. (2004). MicroRNA genes are transcribed by RNA polymerase II. EMBO J. *23*, 4051-4060.

Meyers, B.C., Axtell, M.J., Bartel, B., Bartel, D.P., Baulcombe, D., John L. Bowman,

J.L., Cao, X., Carrington, J.C., Chen, X., Pamela J. Green, P.J., et al. (2008). Criteria for annotation of plant MicroRNAs. Plant Cell *20*, 3186-3190.

Supek, F., Bosnjak, M., Skunca, N., and Smuc, T. (2011). REVIGO summarizes and visualizes long lists of gene ontology terms. PLoS One *6*, e21800.

Trapnell, C., Roberts, A., Goff, L., Pertea, G., Kim, D., Kelley, D.R., Pimentel, H., Salzberg, S.L., Rinn, J.L., and Pachter, L. (2012). Differential gene and transcript expression analysis of RNA-seq experiments with TopHat and Cufflinks. Nat. Protoc. *7*, 562-578.